THE ASTROPHYSICAL JOURNAL SUPPLEMENT SERIES, 66:151–182, 1988 February

PORTRAIT OF A NOVEL NOVA: V1500 CYGNI

CATHERINE M. LANCE
Mount Stromlo and Siding Spring Observatories, Australian National University
MARSHALL L. MCCALL
David Dunlap Observatory, University of Toronto
AND
ALAN K. UOMOTO
Department of Astronomy, University of Texas at Austin
Received 1986 July 29; accepted 1987 August 6

CONTENTS

I. Introduction	152	3–F2
II. Review	152	3–F2
a) Location	152	3–F2
b) Light	152	3–F2
c) Expansion	153	3–F3
d) Extinction	154	3–F4
e) Distance	154	3–F4
f) Absolute Magnitudes and Intrinsic Colors	154	3–F4
g) Dimensions	154	3–F4
h) Systemic Velocity	154	3–F4
i) Temperatures	155	3–F5
j) Densities	155	3–F5
k) Abundances	155	3–F5
l) Mass and Energy of Ejecta	155	3–F5
m) Models	155	3–F5
i) Ejecta	155	3–F5
ii) Central Object	156	3–F6
III. Observations	156	3–F6
IV. Reductions	156	3–F6
V. Measurements	158	3–F8
a) Continuum	158	3–F8
b) Lines	160	3–F11
i) Overview	160	3–F11
ii) The Nebular Template Profile	160	3–F11
iii) Decomposition of Hβ and He II λ4686	160	3–F11
iv) Centroids of the Hβ and He II Remainders	163	3–G1
v) Fluxes and Equivalent Widths of the Hβ and He II Remainders	163	3–G1
vi) N III	163	3–G1
vii) Line Intensities for the Two Components	165	3–G5
VI. Analysis and Discussion	165	3–G5
a) Ejecta	165	3–G5
i) The First 150 Days—Abundances	165	3–G5
ii) Three Years after Outburst	169	3–G9
iii) Filling Factor	170	3–G10
iv) Mass	171	3–G11
v) Ionizing Flux	172	3–G12
b) Central Object	172	3–G12
i) The Binary	172	3–G12
ii) Source of the Ionizing Continuum	173	3–G13
iii) Source of the Optical Continuum	174	3–G14
iv) Source of the Emission Lines	176	4–A2
v) Cause of the Variations	177	4–A3
VII. Conclusions	179	4–A5
Appendix: The Data for the Abundance Analysis	180	4–A6

LIST OF FIGURES

1. Spectrum of 1978 July 16	158	3–F8
2. Grand Mean Spectrum	159	3–F9
3. Flux and Velocity Variations	162	3–F14
4. Line-Profile Variations	164	3–G3
5. Cycle Mean Profiles	165	3–G5
6. Parameterizations of the Profile Variations	167	3–G7
7. Evolution of the Temperature and Density of the Ejecta	169	3–G9
8. The Binary	179	4–A5

LIST OF TABLES

1. Observational Parameters	157	3–F7
2. Observations	157	3–F7
3. Apparent Fluxes and Centroid Velocities	161	3–F13
4. Line Intensities	168	3–G8
5. Atomic Parameters	168	3–G8
6. Physical Parameters for Ejecta	170	3–G10
7. Abundances in Ejecta	170	3–G10
8. Physical Parameters for Binary System	173	3–G13
9. Physical Parameters for Source of Ionization	174	3–G14
10. Components of the Optical Continuum	175	4–A1
11. Phases of Extrema (1978 July 18)	177	4–A3

ABSTRACT

A comprehensive study of the ejecta and remnant of Nova V1500 Cygni 1975 has been performed using previously published observations and heretofore unpublished time-resolved photoelectric spectroscopy acquired 3 years after maximum light. A careful review of previous work indicates that the distance to the nova is 1.2 ± 0.2 kpc, so that the absolute magnitude at peak was $M_V = -10.2 \pm 0.3$. After accounting for errors by past investigators and revisions to critical atomic data, the abundances of carbon, nitrogen, oxygen, and neon in the ejecta were found to be enhanced over the solar values by factors of 20, 60, 8, and 9, respectively, i.e., 1.4–3.0 times less than estimated previously. Yet, the helium abundance was comparable to that in local Galactic H II

regions. The filling factor of the ejecta was substantially less than unity after 1 month, declining with time. The decline pinpoints a source of power for the corona, since it indicates that the self-expansion of constituent clumps was decelerating. The total mass of the ejecta was probably $(5–15)\times10^{-5}$ $M_\odot$. Most likely, the progenitor of the nova was a binary containing an M4 main-sequence star transferring mass to a white dwarf. To model the strength of the outburst with the reduced metallicity and ejecta mass, the white dwarf mass must have been close to the Chandrasekhar limit. However, the enhancements to the carbon, oxygen, and neon abundances are still great enough to suggest that material from the white dwarf core was lost to the envelope either prior to or during the outburst. This material made up about 25% of the ejecta mass. Most of the hydrogen and helium in the ejecta probably came originally from the secondary. Three years after maximum, despite the high metal abundances, the temperature of the ejecta was 11,000 K and the spectrum was dominated by [O III] λλ4959, 5007. This is because the density was still high enough that cooling fine-structure lines were saturated. At this time, the binary contained an accretion disk and a small hot source of ionizing radiation probably associated with it. Most of the optical continuum emanated from the hemisphere of the secondary irradiated by the ionizing source, so that continuum variations were caused by changes in the viewing angle. Significant contributions to the permitted line emission came from both the secondary and the accretion disk. The centroids of Hβ and He II λ4686 varied from -200 km s^{-1} to $+600$ km s^{-1} with a period comparable to that of the continuum, suggesting, in addition, the superposition of a moving component associated with gas passing through a shock at the edge of the accretion disk. The asymmetry in velocity extrema was probably a consequence of the anisotropy in optical depth in the vicinity of the hot spot and the biasing effect of variable low-velocity emission from the secondary.

Subject headings: nebulae: abundances — stars: abundances — stars: novae

I. INTRODUCTION

The first discovery of Nova Cygni 1975 (V1500 Cygni) was made by Osada (1975), who reported a visual magnitude of 3.0 on 1975 August 29. Within one day, the star's brightness rivaled Deneb's. Subsequent investigations showed that the rise to maximum was the most spectacular ever observed for any nova.

Interest in Nova Cygni fell roughly in step with the light curve. In the first year following the outburst, there was a flood of research activity. However, since 1978, very little work has been reported.

Despite the extensive research, significant questions about the nova were never answered. Most important, the nature of the central object remained a mystery. In an effort to unveil the progenitor and identify the origins of the peculiarities of the system, the authors undertook a program of time-resolved photoelectric spectrophotometry 3 years after maximum light. The analysis of these data, reanalyses of earlier observations, and the overall implications for both the ejecta and the central object are presented here.

In § II, research done on V1500 Cygni to date is reviewed, and evaluations are made to determine the most likely values of essential astronomical parameters. The authors' observations and reductions are discussed in §§ III and IV, respectively, and measurement procedures and results are discussed in § V. The properties of the ejecta and the nature of the central object are studied in § VI, and conclusions are presented in § VII.

II. REVIEW

a) Location

The unweighted average of the accurate FK4 positions reported by de Vegt and Gehlich (1975), Isobe *et al.* (1975), and Fischer (1976) is

$$\alpha(1950) = 21^{\rm h}09^{\rm m}52\overset{\rm s}{.}822 \pm 0\overset{\rm s}{.}003,$$

$$\delta(1950) = +47°56'41\overset{''}{.}14 \pm 0\overset{''}{.}13,$$

where the uncertainties represent standard errors. While the individual right ascension estimates agree within the errors (range $0\overset{\rm s}{.}009$), it should be noted that the declination estimate of Isobe *et al.* (1975) is significantly lower (by $0\overset{''}{.}4$) than the other two values.

The corresponding Galactic coordinates are

$$l = 89°49', \quad b = -00°04'.$$

Thus, Nova V1500 Cygni is located in the Galactic plane directly ahead of the orbital path of the Sun.

b) Light

The progenitor of V1500 Cygni was not visible on the Palomar Sky Survey prints (Samus 1975; de Vegt, Gehlich, and Kohoutek 1975; Beardsley *et al.* 1975). Thus, its apparent magnitude was fainter than 21 in the blue and fainter than 20 in the red. Duerbeck (1987) has identified what may be the progenitor at a brightness near the detection limit of the Palomar Sky Survey blue *plate*. Alksne and Platais (1975) and Samus (1975) reported detecting the nova at about magnitude 16 on photographs taken on 1975 August 6 and August 12. Maximum light was reached on

$$T_{\rm max} = 1975 \text{ August } 30.88 \pm 0.02 = \text{JD}_\odot\ 2{,}442{,}655.38 \pm 0.02$$

(Young *et al.* 1976), at which time the apparent magnitude was

$$m_{V,\,\rm max} = 1.85 \pm 0.03$$

(Young *et al.* 1976). The colors at maximum were $(B-V)_{\rm max} = +0.62 \pm 0.01$ and $(U-B)_{\rm max} = -0.15 \pm 0.04$ (Young *et al.* 1976). Fifteen days later, the apparent magnitude was

$$m_{V,15} = 6.80 \pm 0.05$$

(Young *et al.* 1976).

From an analysis of the rate of increase of the infrared flux in three wavelength bands, Ennis *et al.* (1977) determined that the outburst began on

$$T_0 = 1975 \text{ August } 28.5 \pm 0.5 = \text{JD}_\odot\ 2{,}442{,}653.0 \pm 0.5$$

(see also Barnes 1976; Hutchings, Bernard, and Margetish 1978). It appears that the outburst occurred in two stages. In the second stage, the nova brightened by at least 11 mag in only 2 days (Young *et al.* 1976). Relevant photometric time scales, measured by Young *et al.* (1976), are

T_2^* = time to rise 2 mag to maximum light

$= 1.51 \pm 0.02$ days,

T_2 = time to fall 2 mag from maximum light

$= 2.43 \pm 0.04$ days,

T_2 = time to fall 3 mag from maximum light

$= 4.03 \pm 0.08$ days.

No other nova has brightened or faded so rapidly.

The evolution of the V-magnitude is given to within 0.5 mag by

$$V = 3.9 \log (T - T_{\max}) + 2.5 \quad [\sim 1100 > (T - T_{\max}) > 1],$$

where time is in units of days (Tempesti 1979; Patterson 1979). Owing to the effects of line emission, the true continuum was 1–2 mag fainter (see Ferland, Lambert, and Woodman 1986*a*).

On 1975 September 9, Tempesti (1975) discovered a 0.1 mag modulation of the optical light curve with a period of 3.4 hr (Rosino and Tempesti 1977). On September 5, Campbell (1975, 1976) discovered a modulation wave moving through the profile of Hα with the same period. The phenomenon was found to be present as early as August 31 in the profiles of other Balmer and Fe II lines (Hutchings and McCall 1977; see also Jeffers and Weller 1975). Variations with an amplitude of 0.4 mag were seen in the satellite ultraviolet 100 days after maximum light (Wu and Kester 1977). The ultraviolet continuum appeared bluest at the peaks of the modulation (Wu and Kester 1977).

A peculiar aspect of the light variations was that the period decreased with time, by 2% in the first year (see Patterson 1978). However, by 1977, the period had stabilized to 0.139617 days = $3^h 21^m 02\overset{s}{.}9$ (Patterson 1979; Lanning and Semeniuk 1981), yielding the following ephemerides (Patterson 1979):

$$\text{JD}_\odot(\text{maximum}) = 2{,}443{,}369.7028 + 0.139617E, \quad (1a)$$

$$\text{JD}_\odot(\text{minimum}) = 2{,}443{,}369.6391 + 0.139617E, \quad (1b)$$

where E is the number of cycles since the epoch. No other periods over the range from minutes to days were ever found (Semeniuk *et al.* 1977; Patterson 1978; Kemp *et al.* 1979). In particular, early suggestions of a "double period" (6 hr) were probably caused by random variations occurring on time scales of days (Kemp *et al.* 1979).

Lanning and Semeniuk (1981) found that the amplitude of the light variations fluctuated erratically between zero and 1 mag from cycle to cycle (see also Patterson 1979). Random flickering has been observed at all phases ever since outburst (Kemp, Sykes, and Rudy 1977; Patterson 1978, 1979). In 1981 the light variations were still evident, but the period was shorter by 5×10^{-6} days (Kruszewski, Semeniuk, and Duerbeck 1983). In 1987, the photometric behavior resembled that of an AM Herculis object (Chlebowski and Kaluzny 1987).

Most, if not all, of the observed linear polarization was interestellar in origin (McLean 1976; Kemp and Rudy 1976; Efimov, Narizhnaya, and Shakhovskoi 1977; Kemp, Sykes, and Rudy 1977). However, Kemp and Rudy (1976) reported detecting structure in the circular polarization spectrum around Hα, and, in view of the absence of intrinsic linear polarization, suggested that a pole-on magnetic field was responsible. Just recently, it was discovered that the optical light is strongly circularly polarized, and that the polarization is modulated by the 3.35 hr period (Schmidt, Smith, and Elston 1987).

c) *Expansion*

Duerbeck and Wolf (1977) identified the three absorption-line systems characterizing the evolution of novae. Premaximum spectra displayed absorptions at -1400 km s^{-1}. At maximum light, the principal absorption-line system appeared at -1600 km s^{-1}. One day later, the diffuse enhanced absorption was clearly visible at -4000 km s^{-1} (see also Ferland 1977*a*). If a projection factor of 24/17 is applied to the principal absorption velocity, an expansion rate of 2200 km s^{-1} is indicated for the photosphere near maximum light (see Barnes 1976).

The widths of emission lines also measure the expansion velocity of the ejecta. Rosino and Tempesti (1977) found that the mean HWHM of unblended emission lines increased from 900 to 1400 km s^{-1} over the first 2 days following maximum light, before leveling off around 1500 km s^{-1}. This was probably caused by occultation effects. On day 9, the widths of Hβ and Fe II λ5018 were 1750 and 2400 km s^{-1}, respectively, and wings were seen extending to 3000 km s^{-1} from the line centers (Ferland 1980). The difference between the widths of lines originating from different ions was thought to be due to a velocity gradient through the ejecta (Ferland 1980). A large velocity gradient also was required to explain the evolution of radio emission (Seaquist *et al.* 1980).

Using a modification of the Baade-Wesselink method, Barnes (1976) measured the expansion rate of the photosphere just after maximum light to be $0\overset{''}{.}44 \pm 0\overset{''}{.}09$ yr^{-1} (in radius). Becker and Duerbeck (1980) photographically detected emission $1\overset{''}{.}0$ from the nova in 1980, from which an expansion rate of $0\overset{''}{.}25$ yr^{-1} was derived. In 1983, Cohen (1985) imaged a fragmented shell with a radius of $1\overset{''}{.}7$, implying that the rate of expansion was $0\overset{''}{.}23$ yr^{-1}. In 1984 de Vaucouleurs and de Vaucouleurs (1984) photographed an elliptical nebula measuring $3\overset{''}{.}5 \times 2\overset{''}{.}5$ (before correction for seeing). This suggests that the expansion rate was *less than* $0\overset{''}{.}29$–$0\overset{''}{.}40$ yr^{-1}. The difference between the photometric and

imaging estimates could be explained if the emission seen in the photographs had a significant component of velocity along the line of sight and/or if it originated from material that was substantially below the photosphere at the time of maximum light. The tangential velocity of the ejecta is estimated in § II*e* below. Considering all of the available data, the authors adopt an angular rate of expansion of $0''.25 \pm 0''.03$ yr^{-1} for the shell material visible in the 1980s.

d) *Extinction*

Observations of the continuum energy distributions before and after maximum light, the emission Balmer decrement, a Paschen-to-Balmer line ratio, a helium triplet ratio, interstellar absorption-line equivalent widths, and interstellar polarization yielded estimates for $E(B-V)$ ranging from 0.45 to 0.6 (Ferland 1977*b*; McLean 1976; Tomkin, Woodman, and Lambert 1976). Most important, results derived from the physics of nova continuum and line emission are in excellent agreement with those obtained using extrinsic diagnostics of the interstellar medium. Thus, the authors follow Ferland (1977*b*) and adopt $E(B-V) = 0.50 \pm 0.05$. With $R = 3.2$, then $A_V = 1.60 \pm 0.16$ and $A_B = 2.10 \pm 0.21$.

In contrast to the evolution of other novae, an epoch of dust formation was never observed. No jump in infrared fluxes was seen in the first year following outburst (Gallagher and Ney 1976; Kawara *et al.* 1976; Shenavrin, Moroz, and Liberman 1977; Seaquist *et al.* 1980). The 10 μm excess found by Ennis *et al.* (1977) was due to [Ne II] emission at 12.8 μm (Ferland and Shields 1978*a*). The visual light curve showed no evidence for any epoch of dust formation up to day 1070 (Patterson 1979). Inspection of the *IRAS Point Source Catalog* reveals no source at the position of the nova.

The changes in the gradient of the intensities of the four peaks of the Balmer lines (Hutchings *et al.* 1978) were probably caused by radiative transfer effects (Ferland 1978*a*). The V/R ratios observed for [O III] λ5007 after day 82 remained constant to about 10% until day 669 (Hutchings *et al.* 1978), suggesting that little or no intranebular dust formed over this period. The high values of these ratios were probably a manifestation of the density distribution in the ejecta (Hutchings 1979).

e) *Distance*

Distance estimates for the nova have covered from 0.8 to 2.7 kpc (Neff, Smith, and Ketelsen 1978). The authors have chosen to adopt an average of results from three methods:

1. Empirically, it is found that novae have similar absolute magnitudes 15 days after maximum light (Buscombe and de Vaucouleurs 1955; Cohen 1985). Adopting $M_V(15) = -5.60 \pm 0.45$ (Cohen 1985), the apparent distance modulus for Nova V1500 Cygni is $(m-M)_V = 12.40 \pm 0.45$. With $A_V = 1.60$, the corresponding distance is 1.45 ± 0.32 kpc.

2. Measurements of the color excesses and distances for stars in the vicinity of Nova V1500 Cygni (Young *et al.* 1976) showed that the rate of change of A_V with distance is 1.06 ± 0.11 mag kpc^{-1} ($R = 3.2$). It is important that care was taken to choose stars in fields where the background density was comparable to that around the nova. For $A_V = 1.60$, a distance of 1.51 ± 0.22 kpc is implied.

3. The $(V-R)$ color of a stellar atmosphere is observed to be tightly correlated with the surface brightness (Barnes and Evans 1976; Barnes, Evans, and Parsons 1976). Barnes (1976) assumed that the same relation applied to the photosphere of Nova V1500 Cygni near maximum light, and used VR photometry to determine the angular rate of expansion ($0''.44 \pm 0''.09$ yr^{-1}; see above). Adopting a photospheric expansion velocity of 2200 ± 200 km s^{-1}, as indicated by the principal absorption spectrum, the distance is 1.05 ± 0.24 kpc, nearly independent of the extinction.

The first two results are not strictly independent, since they both depend on the extinction. Therefore, it is appropriate to compute the distance to the nova as the mean of distance 3 and the average of distances 1 and 2. The distance which the authors adopt is 1.2 ± 0.2 kpc. The corresponding distance modulus is $(m-M-A) = 10.4 \pm 0.3$. Cohen (1985) estimated the distance to be 1.1 kpc from her measurement of the expansion parallax.

Combining the adopted distance with the adopted angular rate of expansion, the tangential velocity of the visible shell was 1400 ± 300 km s^{-1}. This is substantially lower than the photospheric velocity near maximum light, but close to the radial velocity of 1180 km s^{-1} measured for the ejecta by Cohen (1985), which she used to determine her expansion parallax. The true velocity of expansion of the visible shell could be at most 1800 km s^{-1}, which suggests that the bulk of the shell material was located below the photosphere at maximum light.

f) *Absolute Magnitudes and Intrinsic Colors*

Based on the adopted distance and extinction, Nova V1500 Cygni must have reached an absolute visual magnitude $M_{V,\max} = -10.2 \pm 0.3$ at peak. The corrected colors for this time are $(B-V)_0 = +0.12 \pm 0.05$ and $(U-B)_0 = -0.54 \pm 0.06$ (see Young *et al.* 1976). The absolute magnitude of the progenitor was $M_B > +8.6$ and $M_V > +8.3$ (see Lang 1980), indicating that any main-sequence star in the system had to have a spectral type later than K7 (Schmidt-Kaler 1982; Patterson 1984). White dwarfs have absolute magnitudes fainter than 10 (Green 1980).

g) *Dimensions*

Based on Barnes's (1976) angular rate of expansion, the radius of the photosphere was $0''.0029$ at maximum light. At a distance of 1.2 kpc, this corresponds to 740 $R_\odot$. By 1985, the *photospheric material* should have expanded to a diameter of $9''$, or 0.05 pc.

h) *Systemic Velocity*

The position and distance place the nova at a galactocentric radius nearly identical with that of the Sun. A radial velocity of -14 km s^{-1} would be expected from the combined effects of Galactic rotation and the peculiar velocity of the Sun with respect to the local standard of rest (Mihalas and Binney 1981).

i) Temperatures

Ferland and Shields (1978*b*) found that between 40 and 140 days after outburst the temperature of the He^+–O^{++} zone of the ejecta declined from 9500 to 8400 K (but see § VI*a*[i]). The low temperatures were thought to be a consequence of enhanced metal abundances. Over the first year, the variation in the ratio of He II to He I emission indicated that the color temperature of the central ionizing source rose from below 50,000 to 170,000 K (Ferland 1978*a*; see also § VI*b*[ii]). Observations of line emission from very highly ionized metals (Grasdalen and Joyce 1976; Fehrenbach and Andrillat 1976) demonstrated the existence of a corona with a temperature of $\sim 10^6$ K (Ferland, Lambert, and Woodman 1977).

j) Densities

The analysis of Ferland and Shields (1978*b*) also yielded the electron density in the ejecta. Beyond day 55, the density in the He^+–O^{++} zone declined with time as

$$\log n_e = 7.28 - 2.35 \log [(T - T_0)/100], \qquad (2)$$

where $(T - T_0)$ is the time in days since outburst and n_e is the electron density in cm^{-3} (but see § VI*a*[i]).

To model the evolution of radio and infrared continuum emission from the nova within the first 2.5 years after outburst, Seaquist *et al.* (1980) required a wide shell containing steep velocity and density gradients. Assuming that the emission was due to thermal bremsstrahlung at 10,000 K, a reasonable fit to the data could be achieved with a spherical distribution of matter in which the density varied as a power law in radius,

$$n_e \propto r^{-k},$$

with k between 2 and 3. The velocity and density structure required in the two cases are given by the following expressions (for a distance of 1.2 kpc):

$$\left.\begin{aligned} v(r) &= 4140(r - r_i)/(r_o - r_i) + 180 \\ \log n_e &= 6.57 - 2 \log (v/1000) \\ &\quad - 3 \log [(T - T_0)/100] \end{aligned}\right\} \quad k = 2, \qquad (3a)$$

$$\left.\begin{aligned} v(r) &= 3480(r - r_i)/(r_o - r_i) + 840 \\ \log n_e &= 6.93 - 3 \log (v/1000) \\ &\quad - 3 \log [(T - T_0)/100] \end{aligned}\right\} \quad k = 3, \qquad (3b)$$

where r_i is the inner radius of the shell, r_o is the outer radius of the shell, v is the velocity of expansion in km s^{-1}, $(T - T_0)$ is the time since outburst in days, and n_e is the electron density in cm^{-3}.

k) Abundances

Ferland (1978*a*) found that the helium abundance of the ejecta was close to the cosmic value. However, from an analysis of the emission-line spectrum between days 40 and 140, Ferland and Shields (1978*b*) found that the abundances of carbon, nitrogen, oxygen, and neon were grossly enhanced relative to cosmic values (see § VI*a*[i]). The iron abundance appeared to be normal. Boyarchuk (1977) also found large excesses of carbon, nitrogen, and oxygen from a curve-of-growth analysis of the absorption spectrum observed before and at light maximum. To explain the observations, Ferland and Shields (1978*b*) surmised that the carbon, oxygen, and neon enhancements came from a white dwarf, while the helium and iron came from matter transferred from a companion star. It is likely that the excess nitrogen was synthesized during the outburst.

l) Mass and Energy of Ejecta

The analysis of the radio and infrared observations by Seaquist *et al.* (1980) yielded the following results for the mass and kinetic energy of the ionized hydrogen (for a distance of 1.2 kpc):

$$M(H^+) = \begin{cases} 9.5 \times 10^{-5}\ M_\odot & (k = 2), \\ 10.1 \times 10^{-5}\ M_\odot & (k = 3), \end{cases}$$

$$E(H^+) = \begin{cases} 6.4 \times 10^{45}\ \text{ergs} & (k = 2), \\ 5.5 \times 10^{45}\ \text{ergs} & (k = 3). \end{cases}$$

It must be noted that the calculations apply to a filled pure hydrogen nebula, and must be scaled by the mean molecular weight per electron and the square root of the filling factor to obtain the true totals (see § VI*a*[iv]). The uncertainty in the distance (0.2 kpc) implies that the mass and energy estimates are only accurate to 40% and 75%, respectively.

Based on the observed light curve, the total energy radiated was $>10^{44}$ ergs (Ferland, Lambert, and Woodman 1986*a*). The measures of Hβ fluxes by Ferland and Shields (1978*b*) between days 40 and 140 indicated that the mass of ionized hydrogen fell from 4×10^{-5} to 2×10^{-5} $M_\odot$ over that time, assuming $A_V = 1.60$ and $d = 1.2$ kpc (see § VI*a*[iv]). Considering the observation of neutral oxygen lines (Ferland and Shields 1978*b*), all mass estimates must be considered to be lower limits for the total ejected during the outburst.

m) Models

i) *Ejecta*

Since the time of outburst, noncoronal emission-line profiles have shown four peaks. Boyarchuk and Gershberg (1977) and Hutchings and McCall (1977) were able to model this structure with an equatorial ring and two polar blobs (see Hutchings 1972). Hutchings, Bernard, and Margetish (1978) estimated that the inclination of the system (tilt of the equatorial ring relative to the plane of the sky) was 50°. Seaquist *et al.* (1980) proposed that the high-density optically active material represented substructure within a more extended and tenuous expanding thick shell. The evolution of the infrared and radio emission suggested that the shell was ionization-bounded for the first month after outburst, but was density-bounded subsequently. The coronal line emission may have

been generated by supersonic turbulence within the ejecta (Shields and Ferland 1978), although Ferland, Lambert, and Woodman (1986*a*) doubted that the mechanism could provide enough energy (but see § VI*b*[iii]). Patterson (1979) preferred to ascribe the coronal region to a collision between the principal ejecta and a wind from the central object.

ii) *Central Object*

Efforts to identify the origin of the continuum and line modulations have been based generally upon the premise that the progenitor of the nova was a binary system in which matter was being transferred from a red dwarf (the secondary) to an accretion disk around a white dwarf (the primary). Unfortunately, no model suggested so far has been able to explain satisfactorily all of the observations.

Fabian and Pringle (1977) suggested that the light variations up until period stabilization were caused by the interaction of the secondary with outflowing material (a wind) from the primary. In this model, the interaction sets up a spiral tunnel in the ejecta, and the light varies as the opening of the tunnel sweeps across the line of sight. As the ejecta expand, the scattersphere shrinks and the opening of the tunnel advances, causing the period of modulation to shorten. The model predicted an eventual stabilization of the period as a consequence of the thinning of the ejecta and exposure of the central source. However, it could not account for the continuation of the light modulations beyond that time. Patterson (1978) suggested that one hemisphere of the cool star was heated by the radiation emanating from the primary, and attributed the light variations subsequent to period stabilization to the changing aspect of the secondary.

Campbell (1976) attributed the line-profile modulations to isotropic variations in the ionizing flux from the central object. The variation of phase with velocity in the profiles was explained in terms of light travel times, and was used to estimate the radius of the shell and the time of outburst. However, Hutchings and McCall (1977) found that the temporal evolution of the velocity-phase relation could not be explained in the context of a linearly expanding shell, and preferred to attribute the profile modulations to the effect of a sweeping searchlight. Hutchings, Bernard, and Margetish (1978) also considered a double-searchlight model, but concluded that the single searchlight was most successful at reproducing the observations. However, Ferland (1980) warned that interpretations of the velocity-phase relations are complicated by expansion and shrinkage of the H^+ ionization front and by the velocity gradient in the ejecta, so that the isotropic radiator cannot necessarily be ruled out.

The source of a searchlight might be either an accretion hot spot or the magnetic pole of a white dwarf. In the former case, the initial period decline would have to be explained in terms of a migration of the spot (but see Patterson 1978). In the latter, it would be necessary to attribute the decline to the spin-up of the white dwarf, requiring that the nova explosion knocked the rotation out of synchronism with the orbit. Wu and Kester (1977) attributed the far-ultraviolet light variations to eclipses by the primary of a hot spot in the vicinity of the primary. Hutchings (1979) likened Nova V1500 Cygni to AM Herculis, and suggested a model in which the accretion disk has a nonuniform surface brightness distribution. Photometry, spectroscopy, and polarimetry in 1987 shows that V1500 Cygni is now a polar (Chlebowski and Kaluzny 1987; Schmidt, Smith, and Elston 1987).

III. OBSERVATIONS

Sequences of spectra were obtained on the nights of 1978 July 16, 17, 18, and 21 with the Cassegrain Digicon spectrograph attached to the 2.1 m f/13.6 Struve reflector at McDonald Observatory in Texas. The detector consisted of two silicon diode arrays (Reticons) inside a photoelectric tube with an S20 photocathode (see Tull, Vogt, and Kelton 1979). Each array was composed of 936 diodes, each 30 μm in width. While one array observed a source, the other simultaneously measured the background 21″ away (east or west). To facilitate accurate sky subtraction, a wobble plate was used to periodically switch the source between the two apertures (every 8–50 s). For each array, integrations were co-added and the background was subtracted on-line.

On July 17, 18, and 21, a slit somewhat narrower than two diode widths was used. Adequate sampling of the slit images was achieved by "microscanning" during the exposures, i.e., by periodically offsetting the images by half a diode width (by changing deflection coil currents) and then interleaving the offset and nonoffset observations into 1872 point arrays. By this procedure, it was possible to take better advantage of good seeing and reduce the sensitivity of velocities to guiding errors. The exposure time, i.e., the total time that each diode was integrating on the source, was usually 15 minutes (0.075 cycles of the nova variations). For microscanned data, this meant that each sample (as opposed to diode) represented 7.5 minutes of integration.

A spectrum of a neon-argon discharge lamp was acquired preceding and following every pair of nova observations. An internal continuum lamp was observed during the night to facilitate correction for small-scale response variations. To correct for large-scale response variations, observations of stellar flux standards calibrated by Stone (1977) were made close in time and in space to the nova observations.

Instrumental parameters for the four nights are listed in Table 1. Details of the observations are given in Table 2. Phases have been computed from equation (1a) (Patterson 1979). All together, 26 spectra of the nova were obtained. The 12 spectra acquired on July 18 covered 1.22 cycles, with the first three overlapping the last three in phase.

IV. REDUCTIONS

The two spectra arising from each observation were reduced independently before averaging. A dispersion curve was determined from each discharge spectrum by fitting a fifth-order polynomial to about 30 unblended lines with accurately known wavelengths. Dispersion curves for the nova spectra were derived by linearly interpolating in time the coefficients of the polynomial fits to the encompassing discharge spectra. This was equivalent to interpolating the wavelength of each individual pixel, because all calibration spectra had been fitted with a polynomial of the same order. The nova spectra were corrected for small-scale response varia-

TABLE 1

OBSERVATIONAL PARAMETERS

PARAMETER	UT DATE (1978) July 16	July 17	July 18	July 21
Slit	2″.0×7″.4	1″.7×2″.2	2″.0×2″.2	2″.0×7″.4
Projected slit width (Å)	3.1	1.2	1.4	1.4
Sampling interval (Å)	3.6	0.9	0.9	0.9
Sample widths (Å)	3.6	1.8	1.8	1.8
Samples per spectrum	936	1872	1872	1872
Wavelength range (Å)	3500–6500	4000–5500	3900–5400	3900–5400
Seeing	1″	1″	2″	2″×3″

TABLE 2

OBSERVATIONS

UT Date (1978)	Mean UT	Mean Hour Angle (hhmm)	Exposure (s)	$JD_\odot$ (−2,443,700)	Phase[a]
July 16 ...	1103.5	+0233	608	5.9626	0.445
	1115.5	+0245	608	5.9710	0.505
July 17 ...	0814	−0013	960	6.8449	0.764
	0842	+0014	920	6.8644	0.904
	0903.5	+0037	928	6.8793	0.010
	0928	+0101	928	6.8963	0.132
	0948.5	+0121	928	6.9106	0.235
	1022	+0155	928	6.9338	0.401
	1042.5	+0215	928	6.9481	0.503
July 18 ...	0651.5	−0132	1000	7.7876	0.516
	0713.5	−0111	900	7.8029	0.626
	0736	−0048	900	7.8185	0.737
	0758	−0026	900	7.8338	0.847
	0822.5	−0001	900	7.8508	0.969
	0841.5	+0019	900	7.8640	0.063
	0909.5	+0047	900	7.8835	0.203
	0927.5	+0105	900	7.8960	0.292
	0952.5	+0131	900	7.9133	0.416
	1011.5	+0149	900	7.9265	0.511
	1033	+0210	900	7.9415	0.618
	1057	+0234	900	7.9581	0.737
July 21 ...	0801.5	−0011	900	10.8363	0.352
	0823.5	+0012	900	10.8515	0.461
	0957.5	+0147	1000	10.9168	0.929
	1018.5	+0208	1000	10.9314	0.033
	1048.5	+0238	1000	10.9522	0.182

[a] $(JD_\odot - 2{,}443{,}369.7028)/0^d.139617$.

tions by dividing by an appropriate lamp spectrum for the light. Large-scale response corrections were determined separately for each night from the standard star observations using the flux calibrations of Stone (1977). Mean extinction coefficients for McDonald Observatory were adopted. No correction for coincidence losses was necessary. Additional details regarding reduction procedures are given by Uomoto (1981).

Finally, the two reduced spectra acquired from each observation were averaged with equal weight. The resultant spectra were converted to a common linear wavelength scale by carrying out a running 4-point Whittaker (sinc) interpolation. After verifying that there were no systematic variations in the flux in the [O III] λλ4959, 5007 blend, the spectra were placed on the same absolute flux scale by normalizing the [O III] fluxes to the mean value measured on July 16. The July 16 spectra were believed to be most accurately calibrated absolutely because of the good seeing and the large size of the entrance apertures.

For analysis of weak lines, a "grand mean" spectrum was computed by averaging all of the spectra acquired on July 17, 18, and 21. Weights were assigned according to the ratio of the flux in the [O III] blend to the scatter of local continuum points. The mean spectrum for July 16 is shown in Figure 1. The grand mean, which represents 6^h10^m of exposures (3^h05^m per sample), is displayed in Figure 2.

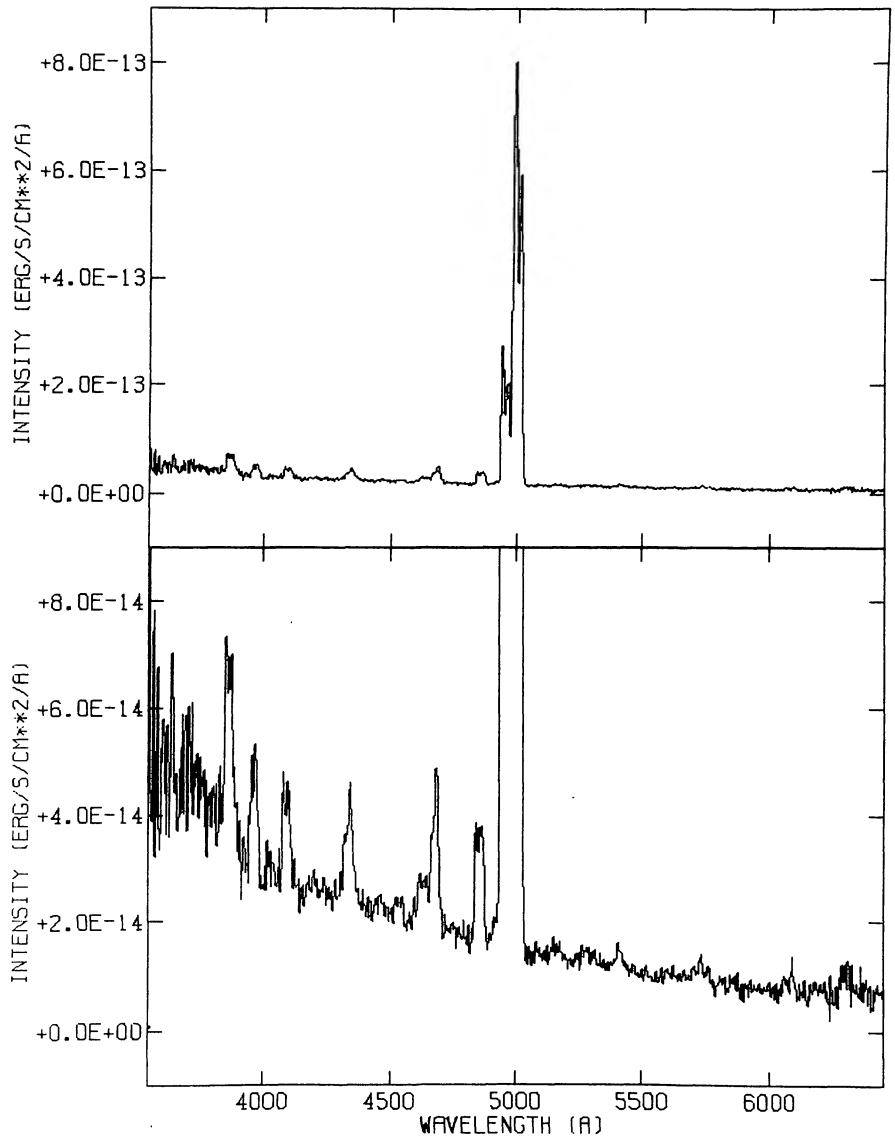

FIG. 1.—Spectrum of 1978 July 16, corrected for extinction $A_V = 1.60$. The dominant feature is [O III] λλ4959, 5007. The presence of neutral clumps is evidenced by [O I] emission at 6300 Å.

Judging from the rms deviation of the fits to the discharge spectra, it is believed that the wavelength calibrations of the high-resolution nova spectra are internally accurate to better than 0.15 Å (0.16 channels). The position of the [O III] blend was measured to vary randomly within and among nights with an rms amplitude of only 11 km s^{-1} (0.20 channels). Because these lines originate in the ejecta, this is probably the best indication of the external accuracy of the relative wavelength calibration. The accuracy of the absolute wavelength calibration could be assessed only through measurements of the positions of the four peaks in the [O III] profiles. From the grand mean spectrum, the velocities were measured to be −945, −510, +150, and +650 km s^{-1} (±10 km s^{-1}). In comparison, Hutchings (1979) measured velocities of −922, −494, +199, and +619 km s^{-1} from data obtained about 20 days later. No systematic difference is evident, suggesting that the absolute accuracy is better than 30 km s^{-1}.

Overall, it is believed that the center-to-end accuracy of relative photometric response corrections is about 5%. Based on the agreement of fluxes and response curves measured for July 16, the absolute accuracy of the response corrections is about 10%.

V. MEASUREMENTS

a) Continuum

Measures of the flux in the continuum were determined for every spectrum by computing the average flux in 50 Å wide bands centered on the spectrophotometric calibration wavelengths 4255 and 4785 Å. Both of these bands were uncon-

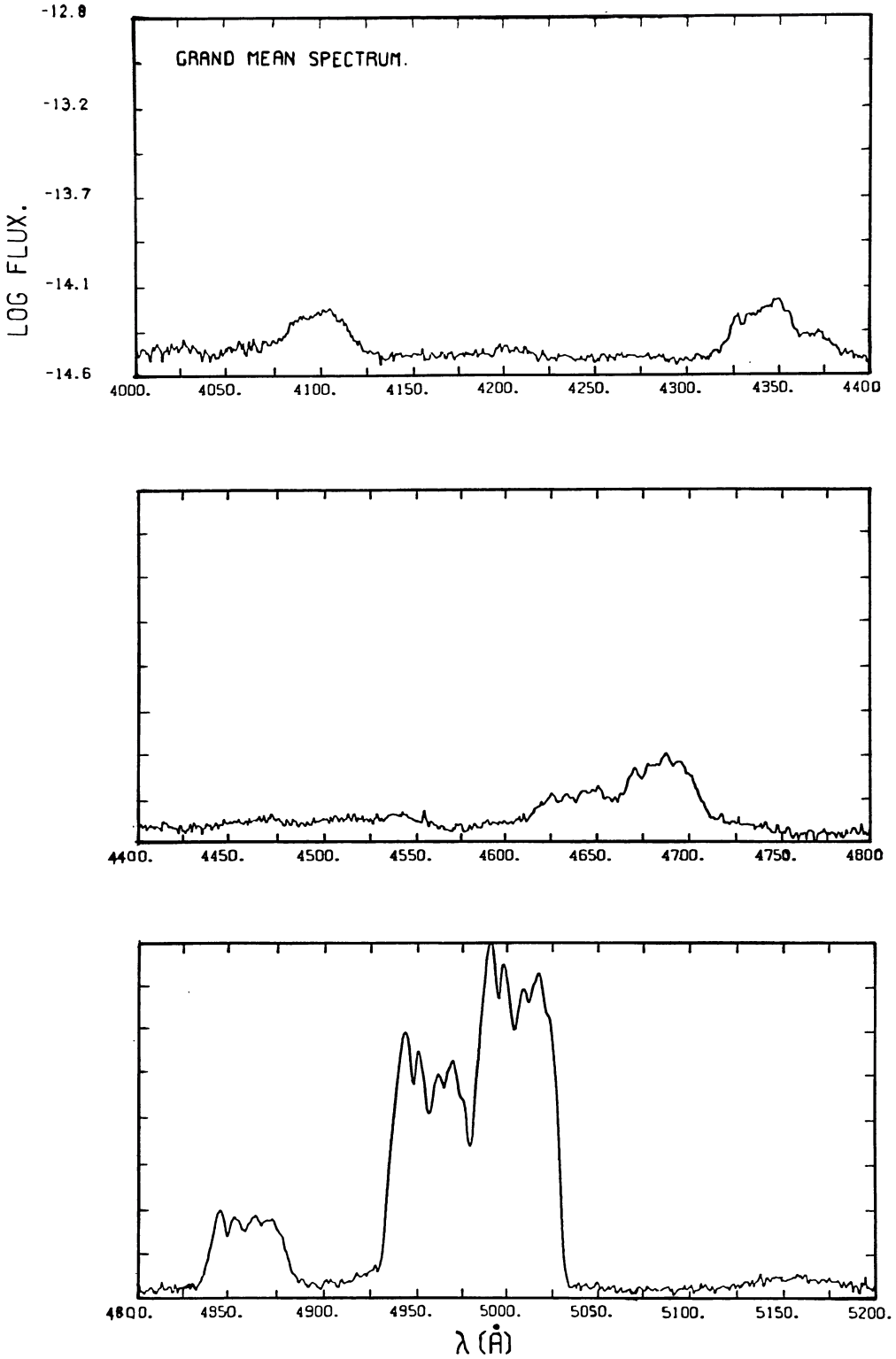

FIG. 2.—Grand mean spectrum, which is a weighted average of all spectra acquired on the nights of 1978 July 17, 18, and 21. No correction for extinction has been applied. To bring out the weakest features, the *logarithm* of the flux is displayed. It should be noted that the blending of N III λ4640 and He II λ4686 has been exacerbated somewhat by the profile variations. Weak neutral helium emission is visible at 4471 Å.

taminated by emission. The results are listed in Table 3. The continuum fluxes measured for July 17, 18, and 21 are plotted against phase (computed from eq. [1a]) in Figures 3*a* and 3*f*. It is estimated that the internal uncertainty of each measurement is about 2%.

The period and phasing of the continuum variations were consistent with the ephemerides of Patterson (1979). In both the 4255 and the 4785 Å bands, maximum and minimum were reached at phases of 0.99 ± 0.03 and 0.55 ± 0.03, respectively. The range of the variation was variable, being greatest (1.0 mag) on July 18. The rise to maximum was steeper than the fall to minimum, consistent with the shape of the mean broad-band light curve constructed by Kemp *et al.* (1979) from data taken during August through October.

A representative color for the continuum was computed from the ratio of the 4255 Å flux to the 4785 Å flux, and corrected for reddening $E(B-V) = 0.50$ using the reddening law of Schild (1977). The corrected color, in magnitudes per unit frequency, is plotted against phase in Figure 3*j*. Based on signal-to-noise statistics, the uncertainty in each value is estimated to be 0.03 mag.

Most of the measurements lie in the range $m_\nu(4255) - m_\nu(4785) = -0.08 \pm 0.03$, indicating that a large portion of the scatter is attributable to observational error. There is no evidence for a systematic variation of color with phase. Furthermore, the color did not change significantly from night to night. It should be noted that for a source this blue, this color index is not a particularly sensitive temperature diagnostic. A temperature change of 2500 K is required to change the color by 0.03 mag. Temperature variations might have been masked also by contributions from nonvariable continuum sources in the system.

A log-log plot of the mean reddening-corrected spectrum for July 16 ($\phi = 0.48$) showed that the continuum could be approximated by a power law between 3500 and 6500 Å. From an eye fit to the continuum points,

$$\log I_\nu = (1.58 \pm 0.13) \log \left(\frac{4785 \text{ Å}}{\lambda} \right) - (24.871 \pm 0.013), \quad (4)$$

where the errors refer to internal uncertainties only. Based on the values of I_ν at the isophotal wavelengths of the B and V bands (see MacFarlane 1969), $(B-V)_0 = -0.146 \pm 0.031$ and $V_0 = 13.81 \pm 0.04$. Thus the apparent magnitude at the time was $V = 15.4$.

b) Lines

i) *Overview*

In 1978 the spectrum of V1500 Cygni was overwhelmingly dominated by [O III] λ4959 and [O III] λ5007 (see Figs. 1 and 2). The only other forbidden lines definitely detected were [Ne III] λ3869, [Ne III] λ3968, and very weak [N II] λ5755 and [O I] λ6300. The latter two identifications were confirmed by a red spectrum acquired on 1979 July 2, in which weak [O I] λ6364 and strong [N II] λλ6548, 6583 were evident also. Most other lines were members of the Balmer series of hydrogen or the Pickering series of singly ionized helium. Neutral helium emission was so weak that it was detectable only in the grand mean spectrum (at 4471 Å). Unblended lines showed the four-peaked structure which has characterized the nova since outburst.

Based on the position of the bluemost peak, the rest wavelength of the feature blended with He II λ4686 is 4640 Å, suggesting that doubly ionized nitrogen is the dominant contributor. This is supported by the observation of N III emission blended with Hδ. In Figure 2 very weak wings can be seen on both the blue and the red side of the N III–He II blend, extending from -4100 km s^{-1} (with respect to N III λ4640) to $+4300$ km s^{-1} (with respect to He II λ4686).

The weak features at 4930, 5170, and 5285 Å are probably the Fe II lines at 4924, 5169, and 5284 Å (Revised Multiplet Table multiplets 42 and 41; Moore 1972). Inspection of the individual slit spectra reveals that the feature at 6080 Å may be spurious.

Emitting material in the immediate vicinity of the central object probably had a density sufficiently high to collisionally de-excite metastable levels, thereby weakening forbidden emission relative to permitted emission. Considering also the structure and stability of the line profiles, it is likely that most of the forbidden line emission orginated from the ejecta. However, Balmer and Pickering series lines must have had significant contributions from both the ejecta and the central object, because the profiles were observed to vary with phase (see § V*b*[iv]). The same applies to He I λ4471, because the grand mean profile is similar to that of He II λ4686. Based on the abundance analysis below (§ VI*a*[i]), 90% of the neutral helium emission must have come from the central object (see § VII*a*[ii]). Because the N III emission arises from continuum fluorescence (Williams and Ferguson 1983), a significant fraction probably originated from the vicinity of the central object.

ii) *The Nebular Template Profile*

In 1978 both the ejecta and the central object were contributing substantially to the emission in permitted lines. It was necessary to separate the two components before any analyses could proceed. No variations in flux or velocity were observed for the forbidden lines, confirming that they originated solely in the ejecta. Ferland and Shields (1978*b*) found that line profiles for different ions had very similar shapes, which demonstrated that the nebula was fairly homogeneous. Therefore, it was justifiable to use a single nebular template profile to separate the spectrum of the ejecta from that of the central object.

The profile of [O III] λ5007 in the grand mean spectrum was adopted as the nebular template. To separate it fully from [O III] λ4959, the blend was placed on a velocity scale, and a copy was blueshifted (to align [O III] λ5007 with the original [O III] λ4959), scaled (to match [O III]λ5007 with the original [O III] λ4959), and subtracted. The value determined for I([O III] λ5007)/I([O III] λ4959) was 2.99, which is very close to the theoretical value 2.88 (Mendoza 1983).

iii) *Decomposition of* Hβ *and* He II λ4686

To study the profiles of Hβ and He II λ4686 in detail, 200 pixel segments of data encompassing the lines were extracted

TABLE 3

APPARENT FLUXES AND CENTROID VELOCITIES

UT Date (1978)	Phase	F_λ(4255 Å) $\times 10^{14}$ (± 0.007) (ergs s^{-1} cm^{-2} Å^{-1})	F_λ(4785 Å) $\times 10^{14}$ (± 0.007) (ergs s^{-1} cm^{-2} Å^{-1})	F(He II remainder) $\times 10^{13}$ (± 0.04) (ergs s^{-1} cm^{-2})	F(Hβ remainder) $\times 10^{13}$ (± 0.04) (ergs s^{-1} cm^{-2})	F(N III total) $\times 10^{13}$ (± 0.04) (ergs s^{-1} cm^{-2})	$V_\odot$(He II remainder) (± 50) (km s^{-1})	$V_\odot$(Hβ remainder) (± 50) (km s^{-1})	$V_\odot$(N III total) (± 50) (km s^{-1})
July 16	0.475	0.348	0.291	0.912	0.479	0.479	...	...	...
July 17 ...	0.764	0.344	0.321	0.412	0.238	0.514	−95	−35	−15
	0.904	0.427	0.371	0.694	0.406	0.551	−88	−75	+120
	0.010	0.393	0.344	0.611	0.242	0.497	−56	−156	+140
	0.132	0.388	0.339	0.586	0.346	0.419	−191	−120	+73
	0.235	0.328	0.334	0.503	0.488	0.467	+45	−45	+91
	0.401	0.279	0.257	0.664	0.476	0.545	+97	+37	+141
	0.503	0.261	0.265	0.730	0.368	0.527	+48	−100	+164
July 18	0.516	0.198	0.178	0.694	0.430	0.423	+476	+725	+67
	0.626	0.213	0.184	0.724	0.502	0.458	+617	+613	+41
	0.737	0.274	0.273	0.839	0.525	0.446	+431	+413	+82
	0.847	0.429	0.388	1.014	0.691	0.709	+223	+205	+17
	0.969	0.521	0.428	0.898	0.619	0.628	+32	+76	+225
	0.063	0.478	0.429	0.960	0.828	0.718	−137	−85	+16
	0.203	0.351	0.309	0.844	0.697	0.558	−202	−184	+57
	0.292	0.298	0.258	0.727	0.577	0.544	−72	−107	−46
	0.416	0.249	0.223	0.717	0.476	0.496	+172	+290	+173
	0.511	0.212	0.180	0.764	0.480	0.426	+294	+436	+137
	0.618	0.245	0.201	0.807	0.539	0.465	+535	+587	+238
	0.737	0.316	0.281	0.875	0.492	0.625	+306	+422	+47
July 21 ...	0.352	0.237	0.231	0.452	0.245	0.481	−59	+30	+63
	0.461	0.243	0.210	0.431	0.229	0.446	+232	+257	−32
	0.929	0.375	0.341	0.640	0.736	0.734	−178	−54	+113
	0.033	0.360	0.332	0.442	0.394	0.551	−273	−56	+22
	0.182	0.316	0.283	0.489	0.190	0.549	+10	−238	+33

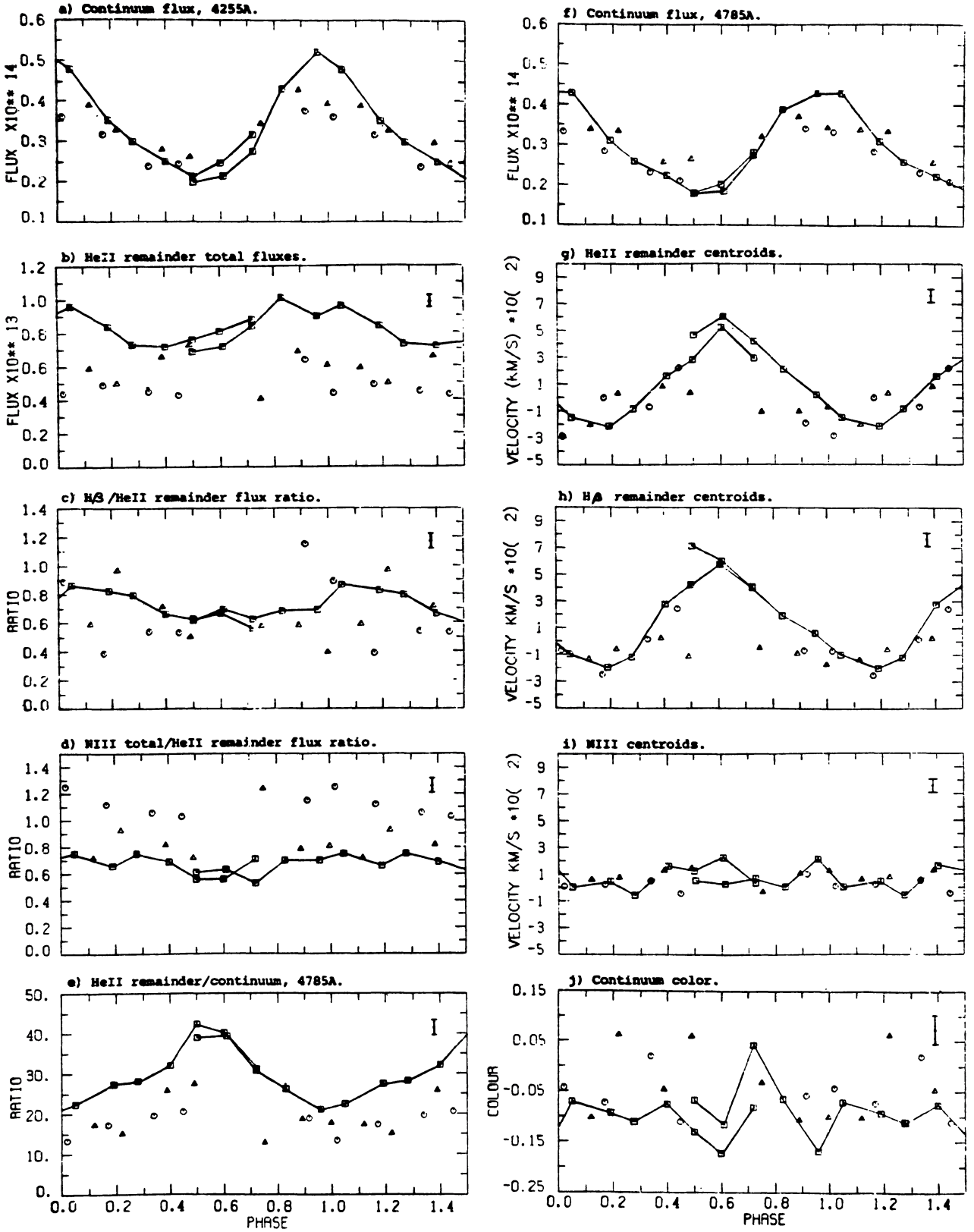

FIG. 3.—Measurements of the flux and velocity variations as a function of phase. In all panels, triangles, squares, and circles mark observations of 1978 July 17, 18, and 21, respectively. To improve clarity, lines have been drawn to connect in time order the observations of July 18. Error bars depict the typical size of random measurement uncertainties. In the case of the continuum fluxes, they are smaller than the symbols. Only the color data in panel *j* have been corrected for reddening. (*a*) Flux in the continuum at 4255 Å (ergs s^{-1} cm^{-2} $Å^{-1}$). (*b*) Flux of He II λ4686 remaining after subtraction of the component due to the ejecta (ergs s^{-1} cm^{-2}). (*c*) Ratio of the remainder fluxes of Hβ and He II λ4686. (*d*) Ratio of the remainder fluxes of N III λ4640 and He II λ4686. (*e*) Ratio of the flux of He II λ4686 to the flux in the continuum at 4785 Å, which is an index of the equivalent width of He II λ4686 (Å). (*f*) Flux in the continuum at 4785 Å (ergs s^{-1} cm^{-2} $Å^{-1}$). (*g*) Velocity of the centroid of the He II λ4686 remainder profile. (*h*) Velocity of the centroid of the Hβ remainder profile. (*i*) Centroid velocity of N III λ4640. (*j*) $m_v(4255) - m_v(4785)$, corrected for reddening $E(B-V) = 0.50$.

from the spectra. The continuum was removed by linearly fitting points on either side of each line. All segments were converted to velocity scales centered on the rest wavelengths of the lines. To remove the N III emission from the He II segments, the mean Hβ profile was scaled down to match the blue side of the N III–He II blend, and then subtracted.

The profiles of Hβ and He II λ4686 showed substantial variations with phase. However, both lines displayed a peaked structure like that of [O III] λ5007, indicating that a substantial fraction of the emission was coming from the ejecta. It was noticed that the blue peaks of the profiles varied least, so were probably least affected by emission from the central object. Therefore, the nebular contribution to the profiles was estimated by scaling the [O III] template down to match the minimum level reached by the blue peaks during the course of the run. This guaranteed that all profiles remaining after subtraction of the nebular components stayed positive. Hanning-smoothed versions of the "remainder" profiles computed for July 18 are displayed in Figure 4. The cycle-mean profiles of Hβ and He II λ4686 for July 18, along with the estimated nebular contributions and the remainders, are displayed in Figures 5*a* and 5*b*, respectively. On July 17 and 21, the flux in the variable component was considerably less, and the remainder profiles were too noisy for detailed study.

iv) *Centroids of the* Hβ *and* He II *Remainders*

The remainder profiles for Hβ and He II λ4686 always appeared similar, but both varied systematically with phase (see Fig. 4). The radial velocities of the centroids are listed in Table 3 and plotted against phase in Figures 3*g* and 3*h*. Sinusoidal variations with the same period but out of phase with the modulation of the continuum are clearly evident. That the velocity shifts are genuinely periodic is evidenced by the good overlap of the measurements for the first and last three spectra of July 18.

The velocity extrema are -200 ± 50 km s^{-1} and $+600\pm50$ km s^{-1}, occurring at phases 0.20 and 0.62, respectively. Most notably, the apparent systemic velocity is $+175$ km s^{-1}.

To help identify the cause of the centroid variations, the fluxes at 200 km s^{-1} intervals of radial velocity within the Hβ and He II profiles of July 18 were plotted against phase, yielding a series of roughly sinusoidal curves. The maximum, minimum, amplitude (defined as half the range of variation), and relative phase shift of each curve are plotted against the velocity within the line profile (relative to the rest wavelength) in Figures 6*a*–6*d*. The amplitude of variation was greatest at -300 km s^{-1} and $+700$ km s^{-1}. A local minimum is visible at $+400$ km s^{-1}. The asymmetry in the activity was responsible for the large systemic velocity seen in the centroid velocity curves.

The results for the velocities are discordant with those of Hutchings (1979). On 1978 August 6, Hutchings found that the He II velocities varied cyclically, but with minimum (0 km s^{-1}) and maximum (700 km s^{-1}) occurring at phases 0.83 and 0.31, respectively (phases computed from eq. [1a]). While the amplitude is in rough agreement with the measurements here (made 19 days earlier), the phases of the extrema appear to be about 0.35 cycles earlier. The mean velocity of the hydrogen lines showed no evidence for any periodic variation. Based on exposure-meter photometry, minimum and maximum light were estimated to have occurred at phases 0.42 and 0.91, respectively, approximately 0.1 cycles earlier than observed here.

Some of the discrepancies may be due to differences in technique. Hutchings derived his velocities by subtracting the *mean* of all of his spectra from each observation and then measuring the positions of the residuals. Thus, the velocities at each phase were perturbed by the emission at other phases present in the mean. Also, the observations suffered from limitations inherent in photographic spectrophotometry. The results for hydrogen may have been a consequence of inadequate signal. Considering these problems, Hutchings's data cannot be used to test reliably the long-term phase stability of the velocity variations.

v) *Fluxes and Equivalent Widths of the* Hβ *and* He II *Remainders*

Remainder profile fluxes are listed in Table 3. The flux in the He II remainder is plotted against phase in Figure 3*b*, and the ratios of the Hβ remainder fluxes to the He II remainder fluxes are shown in Figure 3*c*. The ratio of the He II remainder flux to the flux in the continuum at 4785 Å, which is a measure of the equivalent width of the emission, is plotted against phase in Figure 3*e*.

The He II fluxes were greatest on July 18 (by a factor of 2), at which time they varied roughly in a phase with the continuum. However, the depth of the modulation was only 0.4 mag, considerably less than observed for the continuum. As a consequence, the equivalent width varied strongly, exactly 180° out of phase with the continuum. Yet the changes in equivalent widths from night to night were controlled by the flux in He II. Overall, the observations suggest either that the line and continuum variations were caused by two separate mechanisms or that the sources of line and continuum radiation were not coincident.

On July 18, Hβ/He II varied with phase, ranging from 0.6 to 0.9. However, there were no significant changes in the ratio from night to night, suggesting that the Hβ and He II flux variations were coupled.

vi) N III

The original He II line-profile segments contained N III emission which overlapped slightly with the blue wing of He II λ4686. The contribution by the He II to the blend could be adequately removed by subtracting a scaled Hβ profile. Total fluxes and centroid velocities for the N III profiles are listed in Table 3. The ratio of the total flux to the flux in the He II remainder is plotted against phase in Figure 3*d*. The radial velocities of the centroids of the N III profiles are displayed in Figure 3*i*, and the cycle-mean N III profile is shown in Figure 5*c*.

On July 18 the ratio N III/He II varied little, indicating that the flux in N III was changing pretty much in step with He II. Even though the He II flux was substantially lower on July 17, the ratio was still close to the value observed on July 18. However, the rise in the ratio on July 21 is entirely attributable to the decline in the He II flux. Surprisingly, the centroid of N III on July 18 was fixed at a value of $+70\pm100$ km s^{-1} (relative to a rest wavelength of 4640 Å).

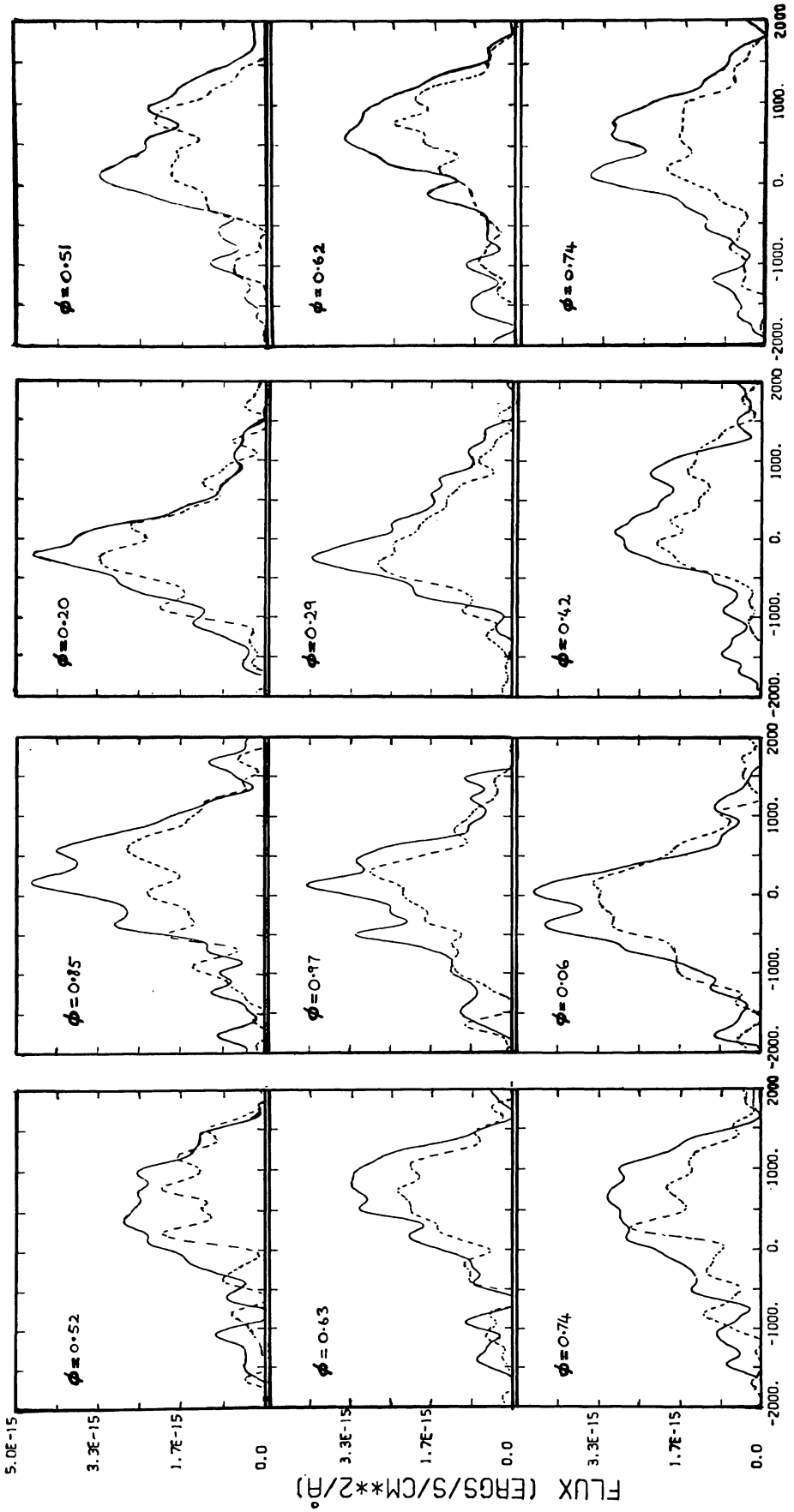

FIG. 4.—Phase dependence of the remainder profiles for 1978 July 18. Abscissae mark velocities relative to the rest wavelength. The solid curves outline He II λ4686, while the dashed curves outline Hβ. All profiles were smoothed with a 9-point Hanning filter. Note the similarity of Hβ to He II λ4686 at all phases.

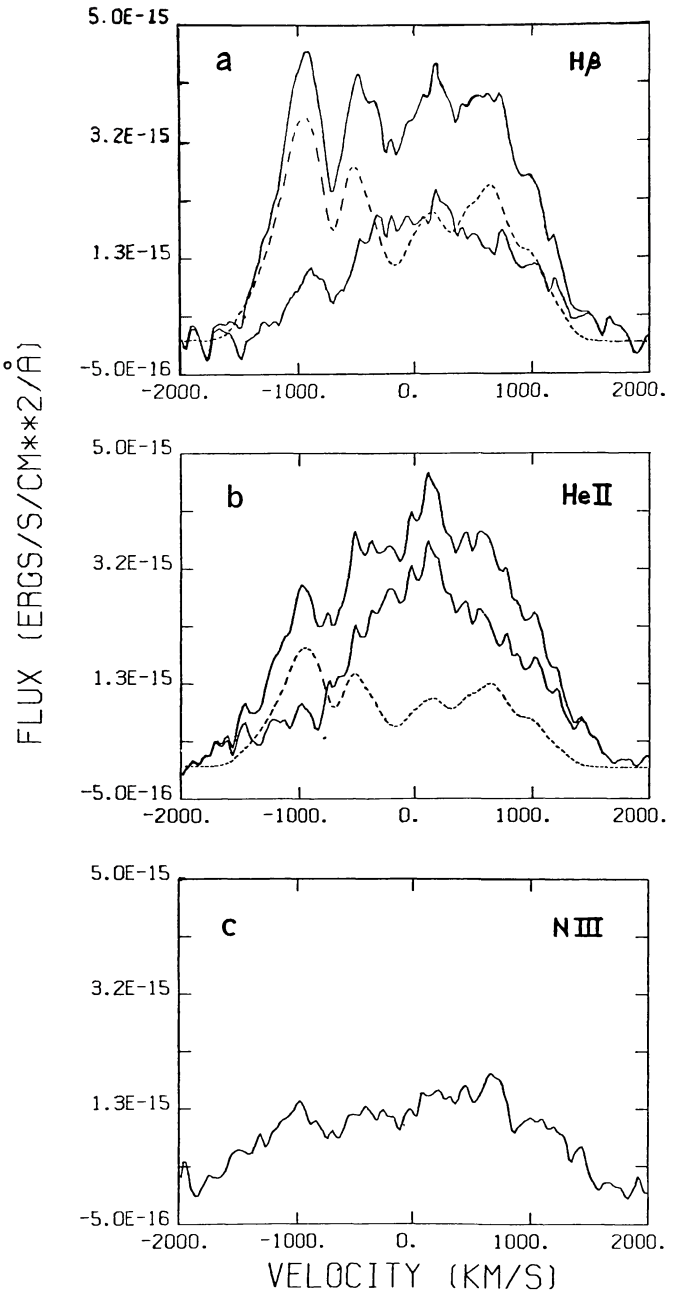

FIG. 5.—Cycle mean profiles for 1978 July 18. Abscissae mark velocities relative to the rest wavelength. (*a*) Hβ. (*b*) He II λ4686. (*c*) N III λ4640. In (*a*) and (*b*), the upper solid curve is the profile before subtraction of the component due to the ejecta, the dashed curve is the scaled [O III] template, and the lower solid curve is the difference.

vii) *Line Intensities for the Two Components*

Because of the greater wavelength coverage, overall characterizations of the spectra of the ejecta and the central object were derived from the mean of the two spectra obtained on July 16. However, important line ratios for the nebula necessary for separating ejecta emission from the central object emission were determined either from analyses of line-profile variations on July 18 ([O III] λ5007/Hβ and [O III] λ5007/He II λ4686) or from the grand mean spectrum ([O III] λ5007/[O III] λ4363) by appropriately scaling the grand mean [O III] template profile. It was assumed that all line emission from the ejecta had the same profile as [O III] λ5007 (see Ferland and Shields 1978*b*).

In order to estimate the central object contribution to the Balmer and Pickering series lines, it was assumed that the reddening-corrected Balmer and Pickering decrements for the ejecta were given by the case B calculations of Brocklehurst (1971) for a temperature of 11,000 K (based on [O III] λ5007/[O III] λ4363; see below) and a density of 10,000 cm^{-3}. Corrections for reddening were accomplished by adopting $E(B-V) = 0.50 \pm 0.05$ and applying the normal Galactic reddening law measured by Schild (1977), which is based on a ratio of total to selective extinction of 3.2. The ratio [O III] λ5007/[Ne III] λ3869 was derived from the July 16 mean spectrum by scaling down a [O III] λ5007 template for those data to match the blue wing of the [Ne III] λ3869–H8 blend. To remove the contribution of [Ne III] λ3968 from the blend with Hε, the reddening corrected intensity of [Ne III] λ3869 was scaled down by a factor of 3.24 (Mendoza 1983) and subtracted. The contribution of hydrogen by the central object to the Hδ–N III blend was determined by interpolating between the reddening-corrected intensities of Hγ and Hε measured for the central object. Then the sum of nebular and central object contributions was subtracted from the total intensity measured for the blend to estimate the strength of N III λ4100. The measurements of the lines and the breakdown into components are presented in Table 4.

It must be noted that Balmer line fluxes include emission from underlying He II Pickering series lines. Based on the Pickering decrements calculated by Brocklehurst (1971), it is estimated that 2.8% of the Hβ flux from the ejecta is due to He II λ4859. In the case of the central object, the strengths of the unblended Pickering lines on either side of Hβ imply that 27% of the Hβ flux is attributable to He II. Both the Balmer and the Pickering decrements for the central object are very shallow compared with case B (in fact, below Hγ the Balmer line strengths appear to increase slightly). These observations suggest that the lines were formed in a region where the density was high and/or the radiation field was intense (Elitzur *et al.* 1983).

VI. ANALYSIS AND DISCUSSION

a) *Ejecta*

i) *The First 150 Days — Abundances*

Helium abundances were computed by Ferland (1978*a*) from measurements of the recombination lines He I λ5876, He I λ6678, and He II λ5412. Ferland and Shields (1978*b*, hereafter FS78) employed observations of [Ne III] λ3869, [O III] λ4363, [O III] λλ4959, 5007, and He I λ5876 from days 42–137 (since T_0) to derive electron temperatures and densities, and then computed metal abundances from line intensity ratios measured on days 42, 79, and 121. Revisions to many atomic constants have been made since the study by FS78. To assess their impact on the abundances, it was decided to repeat the analysis.

Relevant line ratios were extracted from FS78 and Ferland (1978*b*). The latter were recently published by Ferland, Lambert, and Woodman (1986*a*). In the process, several errors were discovered in these works and that of Ferland (1978*a*). The errors and the adopted sources for the *observed* line ratios are summarized in an appendix for the benefit of future workers. A modern high-resolution version of the Galactic reddening law derived by Schild (1977), which differs somewhat from that adopted by FS78 (Miller and Mathews 1972), was used to correct the line ratios for extinction. It was assumed that $E(B-V)=0.50\pm0.05$ (Ferland 1977*b*).

In the temperature-density analysis, three-level atom approximations to the metal ions were used to construct the following three equations for each night (see McCall 1984):

$$\frac{I([\mathrm{O\ III}]\ \lambda\lambda 4959,5007)}{I([\mathrm{O\ III}]\ \lambda 4363)} = C_a t^{u_a} \exp\left(\frac{A_a}{t}\right)\left(\frac{1+Z_{2\mathrm{O}}x}{1+Z_{3\mathrm{O}}x}\right), \quad (5a)$$

$$\frac{I([\mathrm{O\ III}]\ \lambda\lambda 4959,5007)}{I([\mathrm{Ne\ III}]\ \lambda 3869)} = \frac{X(\mathrm{O}^{++})}{X(\mathrm{Ne}^{++})} C_b t^{u_b} \exp\left(\frac{A_b}{t}\right)\left(\frac{1+Z_{2\mathrm{O}}x}{1+Z_{2\mathrm{N}}x}\right) \times\left(\frac{1+L_{\mathrm{N}}x+M_{\mathrm{N}}x^2}{1+L_{\mathrm{O}}x+M_{\mathrm{O}}x^2}\right), \quad (5b)$$

$$\frac{I([\mathrm{O\ III}]\ \lambda\lambda 4959,5007)}{I(\mathrm{He\ I}\ \lambda 5876)} = \frac{X(\mathrm{O}^{++})}{X(\mathrm{He}^{+})} C_c t^{u_c} \exp\left(\frac{A_c}{t}\right)\left(\frac{1+Z_{2\mathrm{O}}x}{1+L_{\mathrm{O}}x+M_{\mathrm{O}}x^2}\right), \quad (5c)$$

where

$$t = T_e/10^4,$$

$$x = 10^{-4} n_e t^{-1/2},$$

$$X(\mathrm{A}^{+i}) = \int n_e n(\mathrm{A}^{+i})\, dV \Big/ \int n_e n(\mathrm{H}^{+})\, dV,$$

and where T_e is the electron temperature, n_e is the electron density, and all other coefficients are constants. A sample of N spectra yields a system of $3N$ equations in $2N+2$ unknowns [$X(\mathrm{O}^{++})/X(\mathrm{Ne}^{++})$ and $X(\mathrm{O}^{++})/X(\mathrm{He}^{+})$, assumed to be time-invariant, and x and t for each epoch], which can be solved by multiple nonlinear least squares.

Mendoza (1983) made a critical compilation of atomic constants relevant to nebular astrophysics, which McCall (1984) used to revise and extend the three-level atom formulae for emission coefficients derived by Seaton (1975), upon which the study by FS78 was based. Incorporated into the revisions were the temperature dependences of collision strengths and five-level atom corrections, which were not considered by FS78. The old and new values of the constants utilized in equations (5a)–(5c) are listed in Table 5. The emission coefficient for He I λ5876 was approximated by a power law in t, based on the results tabulated by Brocklehurst (1972). Changes are mainly due to the revisions to the collision strengths for O^{++}, which resulted from raising the number of target channels used in the close coupling approximation from 9 to 12 (Eissner and Seaton 1974; Baluja, Burke, and Kingston 1981).

The analysis was based upon the 13 observations from days 42–137, which yielded a system of 39 equations in 28 unknowns. The solutions were obtained from a two-step application of multiple nonlinear least squares (to the logarithms), in which the coefficients C_a, C_b, and C_c were corrected to be consistent with five-level atom calculations for the range of temperatures and densities computed. The original and revised solutions for t and $\log n_e$ are plotted against time in Figures 7*a* and 7*b*, respectively. Complete results for days 42, 79, and 121 are listed in Table 6.

The new results for $X(\mathrm{O}^{++})/X(\mathrm{Ne}^{++})$ and $X(\mathrm{O}^{++})/X(\mathrm{He}^{+})$ are 6.26 ± 0.13 and 0.0457 ± 0.0086, respectively, where the errors are the formal uncertainties of the fit. In comparison, FS78 derived values of 6.9 ± 0.4 and 0.130 ± 0.01, respectively. Temperatures are somewhat higher than originally calculated, and remain fairly constant over the term of the observations rather than declining steeply at late times. To a good approximation, the density beyond day 55 falls off as a power law,

$$\log n_e = (7.08\pm0.06) - (2.37\pm0.07)\log\left[(T-T_0)/100\right], \quad 55 < (T-T_0) < 140, \quad (6)$$

where n_e is in units of cm^{-3} and T is in units of days. Densities are systematically lower than estimated by FS78, by about 0.2 dex (see eq. [2]). The formal fit uncertainties in the temperatures and densities are about 200 K and 0.05 dex, respectively.

Residuals for 33 of the 39 points were less than 0.01 dex, and less than 0.02 dex for all but one of the remainder. Increasing $E(B-V)$ by 0.05 led to increases in $X(\mathrm{O}^{++})/X(\mathrm{He}^{+})$, t, and $\log n_e$ of 0.0005, 0.007, and 0.002, respectively, and a decrease in $X(\mathrm{O}^{++})/X(\mathrm{Ne}^{++})$ of 0.3.

Using the old atomic data, it was not possible to reproduce the fit by FS78. Furthermore, the temperatures and densities plotted in Figure 8 of their paper yield results for [O III]/He I λ5876 which are ~ 0.06 dex higher than the observed values, in contradiction to their claim of residuals less than 0.02 dex. It was possible to come very close to their results by changing one digit of one atomic constant (see Table 5). It may be that a typographical error was made in their atomic data file.

The revision to $X(\mathrm{O}^{++})/X(\mathrm{He}^{+})$ indicates that the abundances of oxygen, and, by implication, nitrogen, neon, and iron, must be considerably lower than previously calculated. The helium and metal abundances have been recomputed for days 42, 79, and 121 using the same techniques as applied by Ferland (1978*a*, 1979) and FS78. Following FS78, Hβ self-absorption corrections of 1.30, 1.17, and 1.04, respectively,

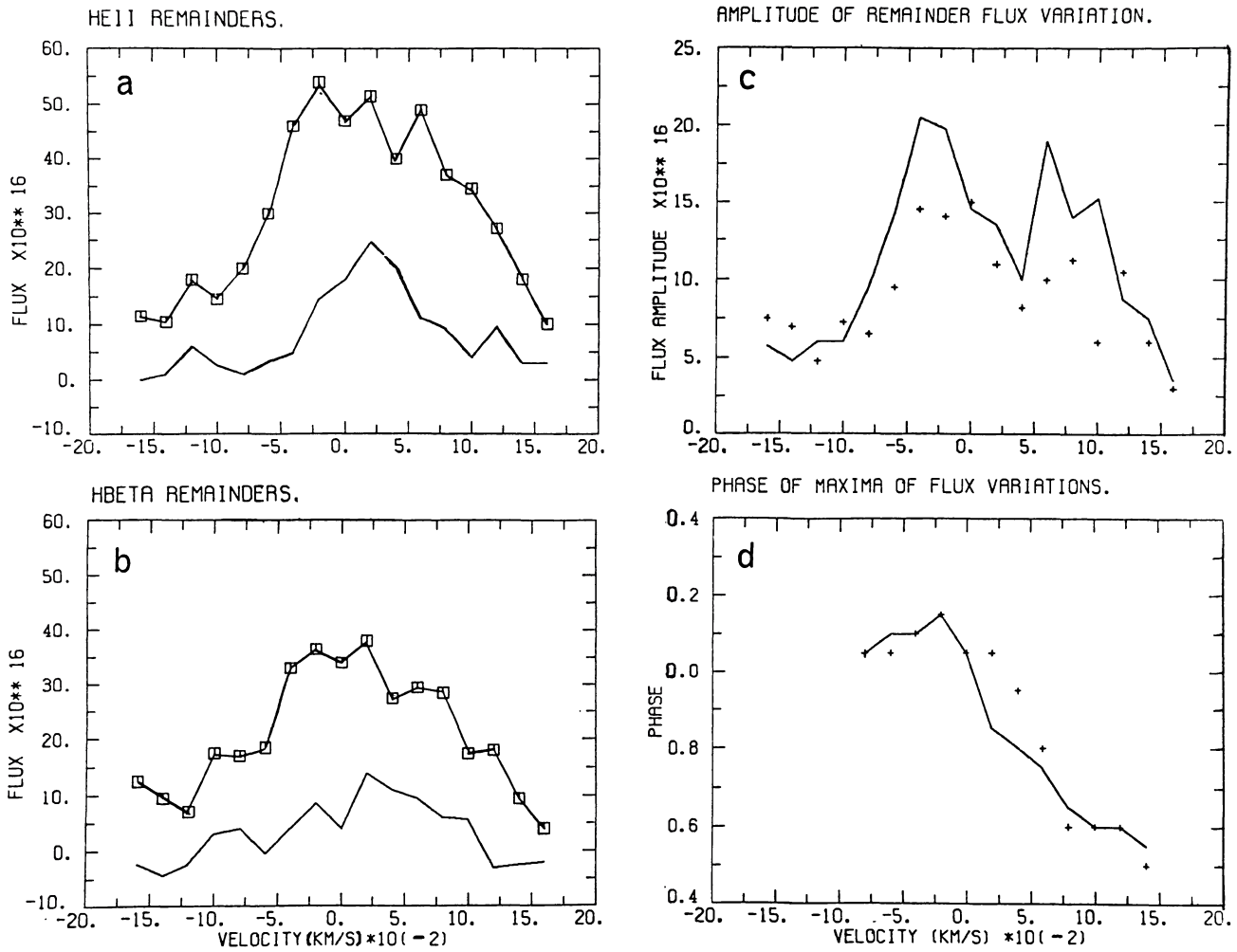

FIG. 6.—Details of the remainder line-profile variations of 1978 July 18. Parameters are plotted against velocity relative to the rest wavelength. (*a*) Maximum and minimum flux within He II λ4686. (*b*) Maximum and minimum flux within Hβ. (*c*) Amplitude of variation (half the range). (*d*) Phase of maximum. In (*c*) and (*d*), the solid lines connect the results for He II λ4686, while the plus signs mark the results for Hβ. All fluxes are in ergs s^{-1} cm^{-2} $Å^{-1}$.

were adopted. Ferland (1978*a*) showed that the effects of radiative transfer and collisional excitations on the neutral helium lines He I λ5876 and He I λ6678 were likely to be small. Emission coefficients for hydrogen and helium were interpolated from Brocklehurst (1971, 1972). To determine the nitrogen, oxygen, and neon abundances, emission coefficients for N^+, O^0, O^+, O^{++}, and Ne^{++} were calculated from a five-level atom program (Binette 1983) incorporating the atomic data compiled by Mendoza (1983) or references therein (for $t=1.0$). To derive the carbon abundance, the effective recombination coefficients listed by Seaton (1978) (for $t=1.0$) were adopted. Dielectronic recombinations do not significantly affect the coefficient for C II λ4267, even though the rate for C^{++} exceeds the radiative recombination rate by a factor of 2.6 (Aldrovandi and Péquignot 1973; Storey 1981). It was assumed that the same is true for C III λ4187. The neon-to-iron ratio was recomputed simply by scaling the FS78 value of ε([Ne V] λ3426)/ε([Fe VII] λ6087) according to revisions in the collision strengths.

Helium and oxygen abundances and important ionization fractions for each of the three nights are listed in Table 6. The old and new mean values for the helium and metal abundances are given in Table 7, where they are compared with those for the solar system (Cameron 1982).

The abundance of oxygen has gone down by a factor of 3.0, and is now only 8 times the solar value. As a result, the abundances of nitrogen, neon, and iron have gone down by similar amounts. A factor of about 1.5 arose from the correction of the errors by FS78, and another factor of 2 resulted from the changes in the atomic data. The value of N/O has risen by 0.15 dex to 7 times the solar value. The carbon abundance is lower by 0.15 dex, but is still enhanced by a factor of 20 over the solar system. The helium abundance has increased by 10%. Although it is 1.8 times higher than the adopted solar value (which is uncertain), the helium abundance is similar to the values found for the novae CP Lacertae and DQ Herculis (Ferland 1979), and is consistent with the "cosmic" value determined from observations of H II regions

TABLE 4

LINE INTENSITIES[a]

λ_0 (Å)	Identification	$A_1(\lambda)$	$15+\log F$[b] (ergs s^{-1} cm^{-2})	$15+\log I$[c] (ergs s^{-1} cm^{-2})	$\log I/I(H\beta)$[c] (ejecta)	$\log I/I(H\beta)$[c] (remainder)
3727.4	[O II]	4.88	<1.17[d]	< 2.14[d]	< −0.57[d]	...
3868.8	[Ne III]	4.71	1.95 (0.03)	2.89	+0.18	...
3889.1	H8	4.69	1.62 (0.13)	2.56	−0.98[e]	+0.04
3967.5	[Ne III]	4.63	1.45[f] (0.03)	2.38[f]	−0.33[f]	...
3970.1	Hε	4.63	1.63 (0.07)	2.56	−0.80[e]	0.00
4097.3, 4103.4	[N III]	4.46	1.32 (0.17)	2.21	...	−0.24
4101.7	Hδ	4.46	1.69 (0.05)	2.58	−0.59[e]	−0.06[g]
4340.5	Hγ	4.26	1.78 (0.03)	2.63	−0.33[e]	−0.18
4363.2	[O III]	4.21	1.55[h] (0.02)	2.39[h]	−0.32[h]	...
4471.5	He I	4.11	0.90[h] (0.05)	1.73[h]	< −0.98[h]	?
4541.6	He II	4.06	1.06 (0.14)	1.87	−1.71[e]	−0.64
4634.2, 4640.6, 4641.9	N III	4.00	1.68 (0.03)	2.48	...	+0.03
4685.7	He II	3.98	2.13 (0.02)	2.93	−0.26	+0.31
4861.3	Hβ	3.84	2.13 (0.02)	2.90	0.00	0.00
4958.9	[O III]	3.74	3.15 (0.01)	3.90	+1.19	...
5006.9	[O III]	3.69	3.63 (0.01)	4.37	+1.66	...
5411.5	He II	3.28	1.40 (0.06)	2.05	−1.36[e]	−0.50
5754.6	[N II]	2.97	1.40 (0.08)	1.99	−0.72	...
6300.3	[O I]	2.71	1.58 (0.11)	2.12	−0.59	...
log (Hβ flux)[b] (erg s^{-1} cm^{-2})	...	...	−12.87 (0.02)	−12.10 (0.02)	−12.29 (0.02)	−12.55 (0.07)

[a] July 16 (phase = 0.48). Center-to-end relative calibration accuracy = 5%, absolute calibration accuracy = 10%.
[b] Uncertainty in parentheses, based on local measurement errors only.
[c] $E(B-V) = 0.50 \pm 0.05$.
[d] Two sigma upper limit, assuming FWHM = 2200 km s^{-1}.
[e] Calculated from Brocklehurst 1971, assuming $T_e = 11{,}000$ K and $n_e = 10^4$ cm^{-3}.
[f] Computed from transition probabilities (Mendoza 1983).
[g] Interpolated from Balmer series.
[h] Measured from grand mean spectrum.

TABLE 5

ATOMIC PARAMETERS

Coefficient	FS78	This Paper
C_a	7.2	7.64[a]
u_a	0.00	−0.05
A_a	+3.30	+3.297
C_b	1.83	1.58[a]
u_b	0.00	+0.13
A_b	+0.823[b]	+0.816
C_c	5.38×10^5	4.86×10^{5}[a]
u_c	+0.61?[c]	+0.73
A_c	−2.90	−2.880
Z_{2O}	5.37×10^{-4}	3.84×10^{-4}
Z_{3O}	6.3×10^{-2}	4.62×10^{-2}
L_O	1.59×10^{-2}?[d]	1.46×10^{-2}
M_O	9.37×10^{-6}	5.49×10^{-6}
Z_{2N}	6.68×10^{-5}	7.09×10^{-5}
L_N	1.11×10^{-3}	1.10×10^{-3}
M_N	6.95×10^{-8}	7.29×10^{-8}

[a] Includes small (~5%) correction based on five-level atom calculations.
[b] Listed as 0.423, a typographical error.
[c] Assuming temperature dependence of He I λ5876 emission coefficient included.
[d] Inferred from efforts to reproduce fit by FS78. The correct value is 1.79×10^{-2}.

located at galactocentric radii comparable to that of V1500 Cygni (Peimbert, Torres-Peimbert, and Rayo 1978).

The random uncertainties in the revised abundances should be comparable to those computed for the old. It is important to note that despite the drastically changing physical conditions, the abundance estimates vary little from day 42 through day 121 (see Table 6). This gives added confidence in the technique of analysis employed. In particular, it confirms that the helium abundances are not significantly affected by collisional excitation or radiative transfer. However, considering the sensitivity of the results to the atomic data for O^{++}, there is still the potential for systematic errors. Because of the uncertainty about conditions in the coronal line region, the apparent depletion of iron must be viewed with caution.

Despite the decreases, the enhancements of carbon, oxygen, and neon abundances in the ejecta remain great enough to imply that material from the core of the white dwarf was mixed with the accreted envelope either prior to or during the outburst, as suggested by Colvin *et al.* (1977) on theoretical grounds. The fact that the helium abundance is close to the cosmic value, despite the mixing, demonstrates that most of the hydrogen and helium in the ejecta came originally from the companion star, and that only a small fraction was involved in nucleosynthesis during the explosion. The authors

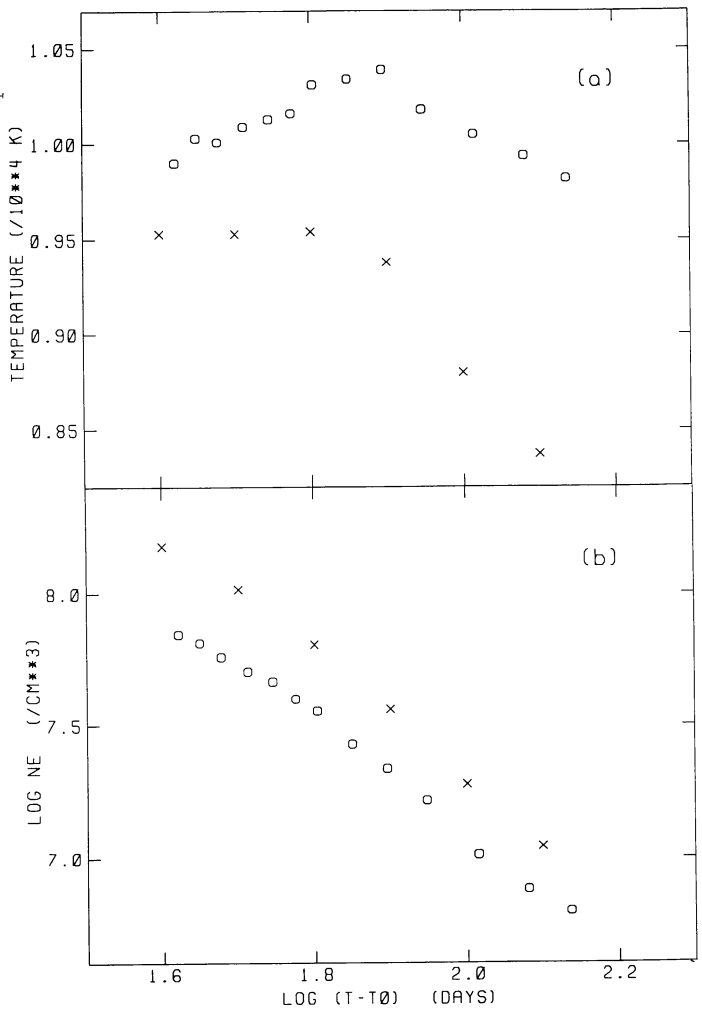

FIG. 7.—Evolution of the ejecta. (*a*) The electron temperature and (*b*) the logarithm of the electron density are plotted against the logarithm of the time since outburst. The crosses show the results of the analysis of Ferland and Shields (1978*b*), and the circles mark the results of this paper. The internal uncertainties in the temperatures and densities are 200 K and 0.05 dex, respectively.

conclude, like FS78, that the bare white dwarf was rich in carbon, oxygen, and neon and deficient in hydrogen and helium. The huge excess of nitrogen in the ejecta suggests that the thermonuclear runaway was powered by the CNO cycle.

ii) *Three Years after Outburst*

The spectrum of the ejecta in 1978 was notable for the great strength of [O III] λλ4959, 5007 relative to the Balmer lines. Here the results of the abundance analysis for 1975 are used to investigate the properties of the ejecta in 1978.

Owing to changes in ionization structure and the possibility of departures from ionization or thermal equilibrium, it is not necessarily valid to assume that ionic abundance ratios in 1978 were the same as in 1975. Therefore, the only way to estimate the density is to extrapolate the decay curve found for the first 140 days. From equation (6) it is estimated that the density in the optical nebula during the 1978 observations (1055 days after outburst) was $\log n_e = 4.65 \pm 0.10$ (cm^{-3}). This implies that the recombination time scale was 3.0 yr (Brocklehurst 1971), which is very close to the expansion time scale. A central source of radiation was not necessarily required to maintain the ionization. The ratio I([O III] λλ4959, 5007)/I([O III] λ4363) was 128 ± 9, indicating that the temperature of the ejecta was $11{,}100 \pm 300$ K (eq. [5a]). This is comparable to the level observed in the first 140 days.

Assuming an expansion velocity of 1400 km s^{-1} (§ II*e*), the radius of the optical nebula in 1978 was about 1.3×10^{16} cm, which corresponds to 120 light-hours. Therefore, since $Q(\mathrm{H}^0) = 5.5 \times 10^{46}$ s^{-1} (see § VI*b*[ii]), the ionization time scale was 1.7 hr. This is sufficiently small compared with the expansion time scale that the ejecta would have adjusted to the decrease in the ionizing flux since 1975. However, it is long compared to the period of the binary, so any modulation wave in the ejecta line profiles (see Hutchings and McCall 1977) would have been smeared. Of course, the wavelength of modulation for such a large nebula is so short (~ 40 km s^{-1}) that it would not have been resolved.

From the estimates for t and $\log n_e$, the values of important ionic ratios have been computed using the same formulae and atomic data employed in the analysis of the 1975 observations. The Hβ self-absorption correction was assumed to be 1.00. The results are given in Table 6. The 1978 measurments of $X(\mathrm{O}^0)$, $X(\mathrm{O}^+)$, $X(\mathrm{O}^{++})$, and $X(\mathrm{He}^{++})$ all indicate that the overall level of ionization of the ejecta increased substantially since 1975. This further suggests that the central source was still ionizing the gas. The presence of [O I] emission shows that ionization-bounded clumps of gas remained, but the low value of $X(\mathrm{O}^{++})$ indicates that 75% of the oxygen in the nebula was more highly ionized than O^{++}. If $X(\mathrm{O}^{++})/X(\mathrm{He}^+)$ were the same as in 1975, then only 13% of the He I λ4471 emission detected could be coming from the ejecta. The true value of $X(\mathrm{He}^{++})/X(\mathrm{He}^+)$ would have been 1.7. Thus, the observations of 1978 would place the oxygen abundance at 0.0036, which is 1.5 times lower than the value calculated for 1975. Considering the size of the ionization correction factor and the uncertainty in the strength of [O II] λ3727 (see below), the agreement is reasonable.

The great strength of the [O III] emission appears to have been due to the combination of a high oxygen abundance and a high temperature. Under normal circumstances (planetary nebulae or H II regions), cooling by [O III] fine-structure lines would lower the temperature and greatly weaken the optical forbidden line emission. However, for V1500 Cygni, the density exceeded the critical values for the $^3P_2$ and $^3P_1$ levels by factors of 12 and 86, respectively, so that the fine-structure lines were saturated, and, relative to the optical lines, less effective coolants (Mendoza 1983). In order to balance the heating by the central object, the temperature of the nebula had to increase to the point that cooling by the optical lines could compensate.

The estimated density and temperature yield a value for $X(\mathrm{O}^{++})/X(\mathrm{Ne}^{++})$ and a lower limit to $\mathrm{N}^+/\mathrm{O}^+$ a factor of 2 greater than were calculated for the first 140 days. Models suggest that both ratios vary little over a wide range of physical conditions (FS78), so it is unlikely that the changes in ionization structure could be responsible. Nor is it likely that dust is responsible. If the discrepancy were due to the

TABLE 6

PHYSICAL PARAMETERS FOR EJECTA

PARAMETER	$T-T_0$ (days) 42	79	121	1055[a]	Notes
t	0.99	1.04	0.99	1.11 ± 0.03	
log n_e(local) (cm^{-3})	7.85	7.34	6.88	4.65 ± 0.10	
$X(O^{++})/X(Ne^{++})$	6.30	6.09	6.34	12.3 ± 1.4	1,2
$X(O^{++})/X(He^{+})$	0.0458	0.0464	0.0460	$>0.0059\pm0.0008$	1,3
$X(N^{+})/X(O^{+})$	...	0.89	0.98	$>2.1\pm0.6$	1
$X(He^{+})$	0.117	0.095	0.097	$<0.215\pm0.025$	1
$X(He^{++})$	0.011	0.018	0.023	0.047 ± 0.004	1
$X(He^{++})/X(He^{+})$	0.098	0.194	0.244	$>0.218\pm0.028$	1
$X(O^{0})$	0.00051	0.00021	0.00008	0.00004 ± 0.00001	1
$X(O^{+})$	0.00024	0.00024	0.00036	$<0.00005\pm0.00001$	1
$X(O^{++})$	0.00480	0.00414	0.00419	0.00128 ± 0.00011	1
n(He)/n(H)	0.128	0.113	0.120	$<0.262\pm0.025$	
n(O)/n(H)	0.00554	0.00523	0.00566	$>0.00162\pm0.00014$	
log r (cm)	14.71	14.98	15.17	16.11 ± 0.09	4
log $L(H\beta)$ (ergs s^{-1})	35.68	35.00	34.39	31.95 ± 0.17	5
log $M(H^{+})$ (g)	28.94	28.80	28.63	28.47 ± 0.20	5
log f	-0.5	-1.1	-1.3	-2.5 ± 0.7	5,6
log $\phi(H^{0})$ (s^{-1} cm^{-2})	17.9	17.3	16.5	13.4 ± 0.6	5,7

NOTES.—(1) $X(A^i)=\int n_e n(A^i)\,dV/\int n_e n(H^+)\,dV$. (2) Nonlinear least-squares solution for 13 nights $=6.26\pm0.13$. (3) Nonlinear least-squares solution for 13 nights $=0.0457\pm0.0086$. (4) Radius of matter moving at 1400 ± 300 km s^{-1}. (5) Based on a distance of 1.2 ± 0.2 kpc. (6) Filling factor, assuming n_e (rms) $\propto r^{-3}$ (Seaquist *et al.* 1980). (7) Flux (by number) of ionizing photons at radius r.

[a]Uncertainties for day 1055 include all known sources of error.

TABLE 7

ABUNDANCES IN EJECTA[a]

ELEMENT	V1500 CYGNI FS78	V1500 CYGNI This Paper	SOLAR SYSTEM Cameron 1982	NOVA MINUS SOLAR SYSTEM
He	11.04 ± 0.04	11.08	10.83	+0.25
C	10.08 ± 0.2	9.93	8.62	+1.31
N	10.04 ± 0.2	9.71	7.94	+1.77
O	10.22 ± 0.1	9.74	8.84	+0.90
Ne	9.38 ± 0.2	8.94	7.99	+0.95
Fe	7.48 ± 0.3	7.14	7.53	-0.39
X	0.49	0.57	0.77	...
Y	0.21	0.27	0.21	...
Z_{CNO}	0.27	0.15	0.013	...

[a]$12+\log n(A)/n(H)$.

formation of dust external to the optical nebula, then 2.3 mag of visual extinction would have been introduced. However, there is no evidence for an effect of this size in other observations (see § II*d*). If the difference were due to formation of internal dust, then the red peaks of the line profiles would have fallen relative to the blue peaks. In the case of [O III] λ5007, this did not occur. In 1978, the ratios 1 to 4 and 2 to 3 agreed to 10% with the values observed from days 82–669 (Hutchings *et al.* 1978).

Part of the discrepancy may be due to errors in measurement. By 1978, [Ne III] λ3869 had become quite weak relative to the continuum, so an error in the placement of the continuum could have a pronounced effect on the derived intensity. The determination of the appropriate level in the vicinity of this line is made particularly difficult by the blending of lines to the blue, which causes an apparent enhancement of the continuum there. It is possible that interpolation of the continuum between the levels on the blue and red sides may have led to an underestimate of the intensity of [Ne III] λ3869 by a factor of 1.25. If [O II] λ3727 were a part of the enhanced background level in the blue, then the true intensity of the line could be as much as 2.8 times larger than the derived upper limit, which was based on the rms scatter of the data in this region. Thus, measurement errors may account entirely for the high value of N^+/O^+, but only partially for the high value of O^{++}/Ne^{++}. The cause of the remainder of the discrepancy is unknown.

iii) *Filling Factor*

Densities derived from optical line intensity ratios depend only upon the details of collisional and radiative processes, and so reflect local conditions within the ejecta. On the other hand, densities derived from total fluxes, such as from radio continuum observations, depict rms conditions, because they depend upon assumptions about geometry and homogeneity. For volumes which are not completely filled with emitting material, n_{rms} is lower than n_{local} (see Osterbrock and Flather 1959).

It is possible to estimate the filling factor for the ejecta of Nova V1500 Cygni by comparing the optical densities derived above with the radio densities derived by Seaquist *et al.* (1980) during the same period. A substantial fraction of the optical emission probably came from material in the nebula photographed by Becker and Duerbeck (1980), Cohen (1985), and de Vaucouleurs and de Vaucouleurs (1984). The tangen-

tial velocity of this material was 1400 ± 300 km s^{-1} (§ II*e*). This is close to the half-width at half-maximum (relative to the mean of the four peaks) of 1200 km s^{-1} observed for the [O III] λ5007 emission profile in 1978, and to the ring velocity of 1700 km s^{-1} estimated by Hutchings, Bernard, and Margetish (1978) from detailed fits to earlier data. It should be noted that the peaks of the [O III] λ5007 profile remained fixed in velocity between 1 month and 3 years after outburst, indicating that the He^+–O^{++} zone did not migrate significantly through the shell. By equations (3a) and (3b), the rms density of this material is given by

$$\log n_{\rm rms} = 6.28 - 3 \log [(T - T_0)/100] \quad (k = 2), \quad (7a)$$

$$= 6.49 - 3 \log [(T - T_0)/100] \quad (k = 3). \quad (7b)$$

Combining equations 6 and 7, the filling factor is given by

$$\log f = \log (n_{\rm rms}/n_{\rm local})^2$$

$$= -1.60 - 1.26 \log [(T - T_0)/100] \quad (k = 2), \quad (8a)$$

$$= -1.18 - 1.26 \log [(T - T_0)/100] \quad (k = 3), \quad (8b)$$

beyond day 55.

Before day 55, $n_{\rm local}$ changed less rapidly, so f declined more steeply with time. Extrapolating the observed densities, it is estimated that the filling factor for the material moving near 1400 km s^{-1} was close to unity near day 30, which is around the time at which Seaquist *et al.* (1980) suggest that the nebula became density-bounded.

Estimates of log f for days 42, 79, and 121 and the extrapolation for day 1055 are given in Table 6, assuming $k = 3$ (favored by Seaquist *et al.* 1980). Considering the uncertainties in the expansion velocity and the density distribution in the ejecta, the results are only accurate absolutely to about 0.7 dex. Also, the results are dependent upon the premise that the radio-infrared continuum was due primarily to thermal bremsstrahlung at 10,000 K, which may be questionable at early times when a significant coronal contribution may have been present (see § VI*b*[iii]).

The fact that $n_{\rm local}$ decreased with time indicates that the clumps within the ejecta were expanding. The decline in the filling factor suggests that their expansion was decelerating (see below), since the He^+–O^{++} zone did not move significantly with respect to the matter in the ejecta (Hutchings *et al.* 1978). To a first approximation, the portion of the nebula to which the filling factor calculations apply can be represented by a number of completely filled expanding zones (clumps) extending from the inner to the outer edge of a thin shell which is expanding outward from the central object. If this shell contained the bulk of the optically active ejecta, the covering factor would roughly equal the filling factor. The filling factor for a system of m clumps each with radius r at time $T - T_0$ is given by

$$f \approx mr^2/[2V(T - T_0)]^2, \quad (9)$$

where V is the velocity of expansion of the shell as a whole. If at this time

$$n_{\rm local} = n_0 (T - T_0)^{-\zeta}, \quad (10)$$

and if the clumps began to expand close to the time of ejection of the shell, then

$$r = 3v(T - T_0)/\zeta, \quad (11)$$

where v is the expansion velocity of the individual clumps at time $T - T_0$. Since $n_{\rm rms} \propto (T - T_0)^{-3}$,

$$f = f_0 (T - T_0)^{-2(3-\zeta)}. \quad (12)$$

Combining equations (9), (11), and (12),

$$\frac{v}{V} \approx \frac{2\zeta f_0^{1/2}}{3m^{1/2}} (T - T_0)^{-(3-\zeta)}. \quad (13)$$

Note that the filling factor is fixed for a system of uniformly expanding clumps (v/V = constant). After day 55, $\zeta \approx 2.37$ (eq. [6]). Thus, for $V = 1400$ km s^{-1} and $k = 3$,

$$v \sim \frac{570}{m^{1/2}} \left(\frac{T - T_0}{100} \right)^{-0.63} \text{ km s}^{-1}, \quad (14)$$

where $T - T_0$ is in days. If the expansion were subsonic, m would have to exceed 3500, since the sound speed in the gas was 14 km s^{-1}.

The decline in v (and, thus, f) with time might have been due to the development of density enhancements or the interaction of the clumps with other clumps or an interclump medium. If the latter, it is possible that the energy dissipated contributed to the powering of the corona (see § VI*b*[iii]).

iv) *Mass*

In calculating the mass of ionized gas, one must be careful to account properly for the distribution of matter in the ejecta (Peimbert and Sarmiento 1984). If a volume S is incompletely filled with clumps with electron density $n_{\rm local}$, then the total mass of ionized material is given by

$$M = \mu_e m_{\rm H} n_{\rm local} Sf = \mu_e m_{\rm H} n_{\rm rms} Sf^{1/2}, \quad (15)$$

where μ_e is the mean molecular weight per electron and $m_{\rm H}$ is the mass of an amu. Using observations of radio and infrared continuum fluxes, Seaquist *et al.* (1980) determined the radial distribution of $n_{\rm rms}$, and thus the total mass, by assuming that the gas completely filled an expanding spherical shell. On the basis of equation (15), the true mass should be lower than their result by a factor $f^{1/2}$. Since f changed with time, the assumption of a constant ionized gas mass after the first month must be questioned.

Independent estimates for the mass of ionized hydrogen can be obtained from the nebular Hβ fluxes. If $L(\rm H\beta)$ is the luminosity of Hβ, then

$$M(\rm H^+) = \frac{m_{\rm H} L(\rm H\beta)}{\varepsilon_{\rm eff}(\rm H\beta)\, n_{\rm local}}, \quad (16)$$

where $\varepsilon_{\rm eff}(\rm H\beta)$ is the emission coefficient for Hβ. Values of $L(\rm H\beta)$ were computed from the observed fluxes (Ferland 1978*b* and this paper) for days 42, 79, 121, and 1055 by adopting a distance of 1.2 kpc, a reddening $E(B-V)=0.50$, the reddening law of Schild (1977), and the self-absorption corrections used in the abundance analysis above. The emission coefficient for Hβ was determined from t and $n_{\rm local}$ by interpolating the tables of Brocklehurst (1971). Results for $L(\rm H\beta)$ and $M(\rm H^+)$ are given in Table 6.

As predicted by equation (15), the masses are lower than $\log M(\rm H^+)=29.4$ (g) estimated by Seaquist *et al.* (1980) (corrected for $n_e \neq n_p$). If $n_{\rm local}$ is replaced by $n_{\rm rms}$ ($k=3$) in equation (16), the values of $\log M(\rm H^+)$ for days 42, 79, 121, and 1055 are raised to 29.17, 29.34, 29.27, and 29.7 ± 0.3, respectively. The good agreement with the radio-IR mass suggests that the high-velocity gas constituted only a small fraction of the total mass of the ejecta. It should be noted that the constancy of the mass with time was forced by the model used to extract $n_{\rm rms}$ from the evolution of the radio and infrared fluxes.

Judging from the behavior of Hβ, the true mass of ionized gas decreased by a factor of 2 between days 42 and 121. The result for day 1055 is slightly lower still, although it is more uncertain because of the density extrapolation involved. If real, the mass decline implies that the clumps contained neutral gas, as had already been suggested by the observation of [O I] lines throughout this period, even though part of the total volume was density-bounded after about 1 month (Seaquist *et al.* 1980). Therefore, estimates for the mass of the ejecta should be regarded as lower limits.

The actual nebula undoubtedly consisted of clumps inside a medium (rather than a near-vacuum), so the above analysis is somewhat oversimplified. Thus, $n_{\rm local}$ probably represents an upper limit to the effective density of material contributing to Hβ, while $n_{\rm rms}$ represents a lower limit. Overall, it is concluded that $28.8 \leq \log M(\rm H^+) \leq 29.2$. Taking into account the composition (Table 7), the total mass of the ejecta was $29.0 \leq \log M(\rm ejecta) \leq 29.5$, or $5\times10^{-5} \leq M(\rm ejecta)/M_\odot \leq 15\times10^{-5}$, provided that the mass of neutral gas was small compared to the mass of the ionized component prior to day 100.

v) *Ionizing Flux*

To estimate the flux of ionizing photons in the ejecta, it is assumed that the ionization was maintained primarily by radiation from a central source. This was probably the case for days 121 and 1055, but perhaps not for days 42 and 79 (see § VI*b*[iii]). Assuming ionization equilibrium,

$$\frac{\Omega}{4\pi} Q(\rm H^0) = \frac{\alpha_B(\rm H^0)\, L(\rm H\beta)}{\varepsilon_{\rm eff}(\rm H\beta)}, \qquad (17)$$

where Ω is the total solid angle subtended by optically thick clumps ($\Omega/4\pi$ is the covering factor), $Q(\rm H^0)$ is the rate of emission of ionizing photons by the central object, and $\alpha_B(\rm H^0)$ is the case B recombination coefficient for hydrogen. A rough estimate for the covering factor is provided by the filling factor (although, in general, it represents a lower limit).

Estimates for the luminosity and radius of the source of ionizing radiation are derived in § VI*b*(ii) below by approximating the covering factor by the filling factor (see Table 9). The values for the ionizing luminosity were used to calculate the number flux of ionizing photons [$\phi(\rm H^0)$] arriving at the gas moving outward at 1400 km s^{-1} (for which the filling factor was calculated). The results for days 42, 79, 121, and 1055 are given in Table 6.

The decline in $Q(\rm H^0)$ and the expansion of the ejecta combined to cause $\phi(\rm H^0)$ to decrease steeply with time. Even so, the time scale for ionization was still less than 2 hr at day 1055.

b) Central Object

i) *The Binary*

The observation of periodic radial velocity variations demonstrates that the central object of V1500 Cygni is probably a binary system. Since the absolute visual magnitude before outburst was fainter than 8.3, the component stars must be either cool main-sequence dwarfs or degenerate. Presuming that the conditions for the explosion were set up by mass transfer between stars, the period of the light and velocity variations demands that the Roche-lobe–filling component be nondegenerate. Any main-sequence star in the system must have a spectral type later than K7 and a mass below 0.6 $M_\odot$ (Schmidt-Kaler 1982; Patterson 1984). At this stage, it is reasonable to presume that the classical model for cataclysmic variables applies, and that the progenitor of V1500 Cygni consisted of a Roche-lobe–filling M dwarf transferring matter to a degenerate companion, probably a white dwarf.

The observed period and limits on the masses of the two stars can be used to estimate limits for important orbital parameters. Assuming that $M_1 \leq 1.4\ M_\odot$ and $M_2 < 0.6\ M_\odot$, then $v_1 < 350$ km s^{-1}, $v_2 < 460$ km s^{-1}, $a < 1.4\ R_\odot$, and $a/c < 3.3$ s (for circular orbits). If the secondary both fills its Roche lobe and follows a mass-radius relation, then the period determines its mass and radius (Warner 1976). The secondaries of cataclysmic variables appear to follow the same mass-radius relation as is observed for the lower main sequence (Patterson 1984). Below 0.8 $M_\odot$, the relation can be approximated by a power law of the form $R_2/R_\odot = \alpha(M_2/M_\odot)^\kappa$, where $\alpha=1.0$ and $\kappa=0.88$ (Patterson 1984). Presuming that the observed period represents that of the binary orbit, then $M_2=0.31\ M_\odot$ and $R_2=0.35\ R_\odot$. The results change by less than 20% if the mass-radius relation of Schmidt-Kaler (1982) is used. The corresponding absolute visual magnitude and spectral type are +11.8 and M4, respectively (Patterson 1984). Using an older mass-radius relation, Hutchings (1979) estimated M_2 to be 0.5 $M_\odot$.

The white dwarfs in cataclysmic variables seem to be concentrated in a fairly narrow mass range (Warner 1976; MacDonald 1983; Patterson 1984). As a result, a correlation between period and mass rato is observed (Warner 1973). The data tabulated by Patterson (1984) suggest that $M_2/M_1 = 0.55\pm0.1$ for V1500 Cygni, so that the mass of the white dwarf is only 0.56 $M_\odot$. If correct, the orbital velocities for the primary and secondary would be 140 and 250 km s^{-1}, respectively. The separation of the two stars would be $a=1.08\ R_\odot$.

Assuming that the angular momentum about the primary of material at the inner Lagrangian point is equal to that of material at the outer edge of the accretion disk (see Warner 1976), then the estimates for M_2/M_1 and a would imply that the equilibrium radius of the disk is $r_{\rm disk} = 0.16\ R_\odot$.

Another estimate for the mass of the white dwarf can be gained from theoretical models of nova outbursts. MacDonald (1983) showed that the speed of a nova depends upon the mass of the white dwarf, the accreted envelope mass prior to thermonuclear runaway, and the chemical composition of the envelope. In particular, he found that a significant enhancement of CNO abundances is required for fast novae, whereas slow novae can arise over a wide range of compositions. Adopting an envelope mass $M_{\rm env} = 3\times10^{-4}\ M_\odot$ and the FS78 metallicity $Z_{\rm CNO} = 0.28$, MacDonald estimated that the white dwarf of V1500 Cygni has a mass of 1.04 $M_\odot$, comparable to estimates for many other nova systems.

However, the revisions to the abundances and the envelope mass have a significant impact on theoretical interpretations of the outburst. With $M_{\rm env} = 1\times10^{-4}\ M_\odot$ and $Z_{\rm CNO} = 0.15$, V1500 Cygni moves into the "slow nova" regime of MacDonald's Figure 9 if the mass of the white dwarf is near 1.1 $M_\odot$. In order to increase the nuclear energy generation time scale relative to the time scale for thermal relaxation, and thereby attain shell source temperatures sufficiently high for a strong outburst, the mass of the white dwarf has to be larger. Taking into account the speed of decline, the principal ejection velocity, the envelope mass, and the value of $Z_{\rm CNO}$, V1500 Cygni appears to have been similar to the fast nova CP Lacertae, for which MacDonald estimated the white dwarf mass to be 1.37 $M_\odot$. It may be that the strongest nova outbursts arise in binaries containing a white dwarf close to the Chandrasekhar limit.

If the mass of the white dwarf of V1500 Cygni were 1.4 $M_\odot$, the orbital velocities for the primary and secondary would be 90 and 400 km s^{-1}, respectively, and the separation of the stars would be $a = 1.35\ R_\odot$. In this case, the equilibrium radius of the accretion disk would be $r_{\rm disk} = 0.29\ R_\odot$. According to the calculations of Flannery (1975), the hot spot should be located somewhat farther in, at $r = 0.23\ R_\odot$.

Considering the uncertainty in the period–mass ratio relation and the extreme nature of the outburst, the calculations based on $M_1 = 1.4\ M_\odot$ may be more reliable. Best guesses for the parameters of the binary system are summarized in Table 8 (see also the discussion below). The white dwarf radius was estimated from the mass-radius relation given by Nauenberg (1972), assuming a mean molecular weight of 2.0.

Unfortunately, because of uncertainties about the details of mixing, it is not possible to decide observationally whether or not any of the accreted mass remained with the white dwarf after the eruption. Thus, it is not known whether or not V1500 Cygni will ultimately become a Type I supernova. However, a rough estimate of the rate at which white dwarf material is lost from the system can be gained if it is assumed that the hydrogen mass fraction for the bare white dwarf is near zero and that only a small fraction of the hydrogen and helium in the envelope was involved in nucleosynthesis during the explosion. Then the ejecta can be considered to consist of matter from the white dwarf diluted by gas accreted from the secondary. If M is the total ejected mass, $M_{\rm wd}$ is the component of the ejected mass mixed in from the white dwarf, and X and X_s are the fractions by mass of hydrogen in the ejecta and the secondary, respectively, then

$$\frac{M_{\rm wd}}{M} \approx 1 - \frac{X}{X_s}. \tag{18}$$

Assuming that the secondary has a solar composition, then, from Table 7, about 25% of the mass of the ejecta must have once been a part of the white dwarf. Thus, if the mean period between outbursts is 10,000 yr (Patterson 1984), matter from the white dwarf must be lost from the system at a rate of $3\times10^{-9}\ M_\odot\ {\rm yr}^{-1}$.

TABLE 8

PHYSICAL PARAMETERS FOR BINARY SYSTEM (best guesses)

P	3.35081 hr	a	1.35 $R_\odot$
i	50°	a/c	3.1 s
$M_{V,1}$	$> +8.3$	$M_{V,2}$	+11.8
Sp$_1$	D	Sp$_2$	M4 V
M_1	1.4 $M_\odot$	M_2	0.31 $M_\odot$
R_1	0.003 $R_\odot$	R_2	0.35 $R_\odot$
a_1	0.25 $R_\odot$	a_2	1.11 $R_\odot$
v_1	90 km s^{-1}	v_2	400 km s^{-1}
$r_{\rm disk}$	0.29 $R_\odot$	$R_{\rm spot}$	0.03 $R_\odot$?

ii) *Source of the Ionizing Continuum*

The emission properties of the ejecta can be used to establish the temperature, size, and bolometric luminosity of the source of ionizing radiation. As discussed in the analyses of §§ VIa(iii) and VIa(v) above, the nebula is approximated by a collection of clumps intercepting a fraction of ionizing radiation (from a central source) roughly equal to the filling factor. Then, from equation (17), the total rate of emission of hydrogen-ionizing photons by the source is given by

$$Q({\rm H}^0) = \frac{\alpha_B({\rm H}^0)\, L({\rm H}\beta)}{\varepsilon_{\rm eff}({\rm H}\beta)\, f}. \tag{19}$$

The color temperature $T_{\rm col}$ and the ionizing surface flux by number $N({\rm H}^0)$ can be estimated from $X({\rm He}^{++})$. Above 4.0 rydbergs, the majority of source photons go into ionizing He$^+$. Recombinations of He^{++} yield a diffuse radiation field which maintains the ionization of hydrogen in the He^{++} zone. Thus, provided that the clumps are optically thick and in ionization equilibrium,

$$\frac{\alpha_B({\rm He}^+)}{\alpha_B({\rm H}^0)}\, X({\rm He}^{++}) \approx \frac{Q({\rm He}^+)}{Q({\rm H}^0)} = \frac{\int_{4.0\ {\rm ryd}}^{\infty} N_\nu(T_{\rm col})\, d\nu}{\int_{1.0\ {\rm ryd}}^{\infty} N_\nu(T_{\rm col})\, d\nu}, \tag{20}$$

where $\alpha_B({\rm He}^+)$ is the case B recombination coefficient for He^{++}, $Q({\rm He}^+)$ is the total rate of emission of photons capable of ionizing He$^+$, and $N_\nu(T_{\rm col})$ is the surface rate of emission per unit frequency at frequency ν. The radius R and

TABLE 9

PHYSICAL PARAMETERS FOR SOURCE OF IONIZATION

PARAMETER	$T - T_0$ (days) 42	79	121	1055[a]	Notes
$\log Q(H^0)$ (s^{-1})	48.4	48.4	48.0	46.7 ±0.7	1,2
$Q(He^+)/Q(H^0)$	0.068	0.110	0.140	0.282±0.024	
$T_{col}/10^5$ K	1.04	1.19	1.30	1.77 ±0.08	
$\log N(H^0)$ (s^{-1} cm^{-2})	26.09	26.30	26.42	26.85 ±0.06	3,4
$\log R$ (cm)	10.6	10.5	10.2	9.4 ±0.4	2,5
$\log L$ (ergs s^{-1})	38.2	38.2	37.8	36.6 ±0.7	2,4,5

NOTES.—(1) Assuming ejecta consist of ionization-bounded clumps, where covering factor roughly equals filling factor. (2) Based on a distance of 1.2±0.2 kpc. (3) Surface flux (by number) of ionizing photons. (4) Assuming a blackbody with $T_{eff} = T_{col}$. (5) Assuming spherical symmetry.

[a]Uncertainties for day 1055 include all known sources of error.

bolometric luminosity L of the source can be computed from $Q(H^0)$, the surface rate of emission of ionizing photons $N(H^0)$, and the value of T_{eff} corresponding to T_{col}.

To carry out these calculations, it was assumed that the source of ionizing photons emitted a spectrum which was both thermal and isotropic. The shape of the continuum indicated that the blackbody approximation may be reasonable for days 121 and 1055, but perhaps not for days 42 and 79 (see the next section). Values of T_{col} and $N(H^0)$ were interpolated from the tables of Hummer and Mihalas (1970). Filling factors and Hβ luminosities were taken from Table 6. Emission and recombination coefficients were derived form the tables of Brocklehurst (1971) and Osterbrock (1974). The characteristics of the ionizing source on days 42, 79, 121, and 1055 are summarized in Table 9.

The color temperatures for days 42, 79, and 121 are consistent with the results of Ferland (1978*a*), which were derived from $X(He^{++})/X(He^+)$. Over the first year, the color temperature rose from below 0.5×10^5 K near maximum to about 1.7×10^5 K. Judging from the 1978 result, it leveled off at 1.8×10^5 K. The bolometric luminosity was steady at about 1.5×10^{38} ergs s^{-1} from day 42 to day 79, but had begun to decline by day 121. In comparison, the bolometric luminosity near maximum light was $\sim10^{39}$ ergs s^{-1} (Ferland, Lambert, and Woodman 1986*a*, corrected to 1.2 kpc). Assuming that the opacity was dominated by electron scattering, the Eddington limit (for $M_1 = 1.4\ M_\odot$ and $\mu_e = 1.27$) was 2.2×10^{38} ergs s^{-1}. This suggests that the source may have been losing mass up to about day 100.

By day 42, the source radius had already shrunk to less than half the separation of the two stars. On day 1055, the radius was only 0.035 $R_\odot$, which is about one-tenth of the equilibrium radius of the accretion disk. If the covering factor were larger than the filling factor, the size would be even smaller. For example, adoption of a covering factor equal to the filling factor on day 121 reduces the result for day 1055 to 0.009 $R_\odot$. At minimum, with the covering factor equal to unity, $R = 0.002\ R_\odot$, which is roughly the radius of the white dwarf. It appears that the bulk of the ionizing radiation on day 1055 was coming either from the environs of a hot spot on the perimeter of the disk or from the immediate vicinity of the white dwarf, but probably not from the white dwarf itself.

Next to the covering factor, the most uncertain aspect of the above analysis is the shape of the ionizing spectrum. To assess the impact of the blackbody approximation, calculations for days 42 and 121 were repeated using plane-parallel LTE model atmospheres for the central stars of planetary nebulae calculated by Hummer and Mihalas (1970). Adopting the series 200 (metal abundances roughly one-half solar) atmospheres calculated for $\log g = 5.5$, the results for T_{col}, $\log N(H^0)$, $\log R$, and $\log L$ for day 42 changed by $+0.11\times10^5$ K, +0.14 dex, −0.07 dex, and +0.04 dex, respectively. The results for day 121 changed by -0.05×10^5 K, −0.09 dex, +0.04 dex, and +0.02 dex, respectively. The effect on the luminosities was small because the changes in T_{col} and $N(H^0)$ were partially offsetting. Provided that the ionization of the ejecta was maintained primarily by an optically thick source in the binary (as believed for days 121 and 1055), it appears that atmospheric details need not be known precisely for estimating the radius and luminosity.

iii) *Source of the Optical Continuum*

The optical continuum has been seen to vary with a period of roughly $3\frac{1}{3}$ hours ever since outburst. During the 1978 observations, the peak-to-peak amplitude reached as high as 1.0 mag. Before it becomes feasible to identify the cause of the variations, it is necessary to determine where the continuum originated. This is now possible with the analyses of the ejecta and ionizing source having been completed.

In the first year, the level of the optical continuum was difficult to determine because of the rich emission-line spectrum of the ejecta. However, a narrow region around 4800 Å appears to have been free of line contamination over much of the course of the nova's evolution (Ferland, Lambert, and Woodman 1986*a*; see also Fig. 2). Observations of the luminosity at 4800 Å [Ferland, Lambert, and Woodman 1986*a*, and Fig. 3*f* of this paper, corrected for $E(B-V) = 0.50$] relative to the ejecta Hβ luminosity (Table 6) are listed for days 42, 79, 121, and 1055 in Table 10.

The contribution of the ejecta to the optical continuum at 4800 Å was comprised mainly of bound-free and free-free emission from hydrogen and helium, and, once densities were sufficiently low (e.g., 1978), the two-photon continuum of

TABLE 10

COMPONENTS OF THE OPTICAL CONTINUUM[a]

COMPONENT	$T-T_0$ (days) 42	79	121	1055
Ejecta	2.0	2.2	2.2	3.2–3.6
Source of ionization[b]	1.0	3.1	4.0	33
Sum	3.0	5.3	6.2	36
Total observed	8.1	10.6	12.5	100–240
log L_ν (excess) (ergs s^{-1} cm^{-2} Hz^{-1})	21.6	20.9	20.4	19.0–19.5

[a] $\nu L_\nu(4800\ \text{Å})/L_{\text{ejecta}}(\text{H}\beta)$.
[b] Assuming a blackbody spectrum.

hydrogen. The luminosity of each component relative to the ejecta Hβ luminosity was computed by dividing the volume emission coefficient by $\varepsilon_{\text{eff}}(\text{H}\beta)$ and, in the case of helium, multiplying by $X(\text{He}^+)$ or $X(\text{He}^{++})$ (Table 6). Emission coefficients were estimated from the observed temperatures and densities (Table 6) by interpolating the tables of Osterbrock (1974). The total luminosity of the components relative to Hβ is listed in Table 10.

In order to estimate the contribution of the source of ionizing radiation to the optical continuum, it was assumed (as before) that the spectrum could be approximated by that of a blackbody. The color temperature and radius (Table 9) were used to derive the luminosity at 4800 Å. The results (relative to the ejecta Hβ luminosity) are given in Table 10. It should be noted that, owing to the uncertainty in the covering factor, these estimates may only be accurate to a factor of 4.

In Table 10 it can be seen that the observed continuum was stronger than the sum of the ejecta and ionizing source contributions at all four epochs. The discrepancies amount to factors of 5.1, 1.7, 1.6, and 1.9–6.2 times the contribution of the ionizing source on days 42, 79, 121, and 1055, respectively. The factors for day 1055 change to 2.5–5.1 if the contribution by the source of ionization is varied in proportion to the remainder flux of He II λ4686 (Fig. 3*b*). While the reality of the discrepancies for days 79 and 121 may be questioned considering the uncertainties, the excesses on days 42 and 1055 are probably genuine.

In addition to indications of an excess, Ferland, Lambert, and Woodman (1986*a*) found that the optical-infrared continuum was flat ($I_\nu \propto \nu^{-0}$) from about day 10 to about day 100, but then steepened to a Rayleigh-Jeans tail ($I_\nu \propto \nu^{-2}$) by day 368. They suggested that a substantial fraction of the continuum observed up to about day 100 was due to thermal bremsstrahlung emission from a hot corona, and that after about 1 year, the coronal continuum had faded to the point that thermal radiation from the central object was dominant. Of course, another source of continuum was still required throughout the decline to account for the 3 hr variation. It was estimated that the luminosity of the corona on day 35 was 8×10^{38} ergs s^{-1} ($d=1.2$ kpc). If this is correct, it is possible that the ionization of the ejecta at this time was maintained primarily by coronal radiation (Ferland, Lambert, and Woodman 1986*a*; see also Table 9). The power supply for the corona could not be identified.

One possible source of power for the corona is the interaction of the clumps in the ejecta either with other clumps or with an interclump medium. It will be recalled from § VI*a*(iii) that the decline in the filling factor with time suggested that the self-expansion of the clumps was decelerating. On the basis of equations (12) and (13), the rate of kinetic energy dissipation is given by

$$\frac{dK}{dt} = -\frac{4MV^2 f_0}{9m}\zeta^2(3-\zeta)(T-T_0)^{2\zeta-7}, \qquad (21)$$

where M is the mass of decelerating gas, V is the outward velocity of expansion of the shell, m is the number of clumps, $(T-T_0)$ is the time since outburst, and f_0 and ζ are defined by equations (10) and (12), respectively. Adopting $M=1\times10^{-4}\ M_\odot$ and $V=1400$ km s^{-1},

$$\frac{dK}{dt} = (2.0\times10^{38}\ \text{ergs s}^{-1})\frac{f\zeta^2(3-\zeta)}{m}\left(\frac{T-T_0}{100}\right)^{-1}, \qquad (22)$$

where f is the filling factor and $(T-T_0)$ is in days.

On day 35, $\zeta=1.49$ and $f=0.63$, so $mdK/dt=1.2\times10^{39}$ ergs s^{-1}. Thus, if the effective value of m were not too large, the deceleration of the clumps might well have contributed a significant amount of power to the corona. However, since $m^{1/2}v=11000$ km s^{-1} (eqs. [12] and [13]), the velocities involved would have to have been supersonic.

On day 42, $\zeta=1.49$ and $f=0.36$, so $mdK/dt=5.8\times10^{38}$ ergs s^{-1}, while by day 121, $\zeta=2.37$, $f=0.052$, and $mdK/dt=3.1\times10^{37}$ ergs s^{-1}. If the luminosity of the corona at 4800 Å was in fact related to the rate of dissipation of kinetic energy, one would predict that the excess in the optical continuum on day 121 would be 5% of that observed on day 42. The observed excess was 6% of that on day 42 (see Table 10). The coronal contribution to the continuum on day 1055 should have been a factor of 6–19 times less than the observed excess. Considering the size of the excess and the continuum slope (eq. [4]), it is clear that on day 1055 the bulk of the continuum, and by implication the continuum variations, originated from neither the corona nor the ionizing source.

Estimates for the temperature of the "extra" component at minimum and maximum light on day 1055 (1978 July 18) were derived from the continuum excesses at 4255 and 4785 Å. On the basis of Figure 3*j*, it was assumed that the reddening-corrected color at both minimum and maximum light was $m_\nu(4255)-m_\nu(4785)=-0.12\pm0.03$ (with an additional uncertainty of 0.02 due to the reddening). The extrema of the light curves at 4255 and 4785 Å (Figs. 3*a* and 3*f*) were rounded to be consistent with this color. After subtraction of the contributions from the ionizing source (assumed to be fixed, with $T_{\text{eff}}=1.8\times10^5$ K) and nebula (excluding corona), the colors at minimum and maximum light become -0.06 and -0.10, respectively. The corresponding color temperatures are $14{,}000\pm2000$ K and $17{,}000\pm3000$ K, respectively, where the errors show the effect of the uncertainty of 0.03 mag in the observed colors. The revised peak-to-peak amplitude of the continuum variations is 1.3 mag. For reference, the colors of an infinite alpha disk ($I_\nu \propto \nu^{1/3}$) and an M4 V star are -0.04 and $+1.2$, respectively (Beall *et al.* 1984; Jacoby, Hunter, and Christian 1984).

The radius of this "cool" component is given by

$$R_{\rm cool} = \left[\frac{d^2 I_\nu}{\pi g B_\nu(T_{\rm cool})} \right]^{1/2}, \quad (23)$$

where d is the distance, I_ν is the continuum flux at some frequency ν, $B_\nu(T_{\rm cool})$ is the corresponding surface brightness for temperature $T_{\rm cool}$, and g is a geometrical factor whose value is unity for a sphere and cos i for a disk at inclination i. If the cool component was spherical, its radius would be $R_{\rm cool} = 0.31$–$0.47\ R_\odot$, where the lower estimate refers to minimum light. These values encompass the radius of the secondary ($0.35\ R_\odot$). If it was an optically thick disk inclined 50° to the plane of the sky, then $R_{\rm cool} = 0.38$–$0.59\ R_\odot$, which is substantially larger than the equilibrium radius of $0.29\ R_\odot$ (see also the next section). Considering the random uncertainty in the continuum colors (± 0.03), the precision of estimates for $R_{\rm cool}$ is about 20%. Evidently, the cool component was a large element of the binary system. At maximum, the bolometric luminosity $L_{\rm cool}$ was 8–15 $L_\odot$ [$(3$–$6)\times 10^{34}$ ergs s^{-1}], depending on the geometry, which is 150 to 75 times less than the luminosity of the source of ionizing radiation.

If an accretion disk contributed the bulk of the optical continuum, then the temperature structure would have to have been unusual. For an alpha disk, the temperature varies with radius as $r^{-3/4}$ (Beall *et al.* 1984). The superposition of Planck curves leads to a flat continuum $I_\nu \propto \nu^{1/3}$, such as is observed for the old nova V603 Aquilae (Ferland *et al.* 1982). The cool optical continuum of V1500 Cygni was definitely steeper than this at maximum light on day 1055. If an optically thick accretion disk were responsible, the slope ($I_\nu \propto \nu^{+0.75}$) would suggest that the temperature varied as $r^{-0.89}$ (Beall *et al.* 1984). However, it is difficult to see how continuum variations with the observed amplitude could arise from an accretion disk or its environs when the inclination is only 50°. Heating by radiation from a hot spot would tend to flatten, rather than steepen, the continuum.

The shape of the cool continuum, the amplitude of the variations, and the size of the cool component suggest instead that the *secondary* contributed the bulk of the optical continuum on day 1055. Now, two important questions are raised. First, how could an M4 V star come to look like a B star? Second, why were no absorption lines apparent?

The shape of the continuum from the secondary probably was a consequence of irradiation by the hot source of ionizing radiation. The secondary would appear to cover 2.4% of the sky as seen from the closest point of the equilibrium accretion disk, and 1.5% of the sky as seen from the center of the disk (see Table 8). Thus, the secondary could intercept 10×10^{34} ergs s^{-1} if the ionizing source were located at the nearest edge of the disk, or 6×10^{34} ergs s^{-1} if the ionizing source were at the center of the disk (see Table 9). The luminosity estimated above for the cool component was close to these values. If all of the energy were processed by the facing hemisphere of the secondary, then the apparent temperature of that hemisphere would be 23,000–26,000 K. That the observed temperature (based on the slope of the optical continuum) was somewhat lower is not surprising, since some of the energy from the ionizing source would have been blocked by material in the vicinity of the accretion disk, and some of the energy reaching the secondary would have been convected to the unilluminated hemisphere. Furthermore, the inclination was such that a significant fraction of the cool hemisphere was always visible.

The energy redistribution and the low inclination of the binary probably account for the absence of spectral features characteristic of cool stars. A large fraction of the irradiated hemisphere was visible at all phases. One would have expected to see line *emission* rather than line absorption from this hemisphere, since the temperature gradient would have been inverted. Thus, the line spectrum of the secondary is probably contained within the remainder hydrogen and helium emission profiles.

iv) *Source of the Emission Lines*

The 1978 line spectrum remaining after subtraction of the ejecta background was derived in § V*b* (see Table 4). The Balmer series of hydrogen and the Pickering series of helium were identified. Both the Balmer and Pickering decrements were shallower than expected for case B recombinations, suggesting that the lines originated predominantly from a region where the density was large and/or the radiation field was intense. As discussed in §§V*b*(i) and VI*a*(ii), most of the neutral helium emission of 4471 Å probably came from the same place.

The profiles of Hβ and He II λ4686 changed with time (see Figs. 4 and 6). On July 18, both the fluxes and centroid velocities appeared to vary with a period close to that observed for the continuum (see Fig. 3). The centroid of N III λ4640 remained fixed, but over the course of a cycle the flux varied in step with He II λ4686.

The conditions for formation of the emission lines could exist only within the binary. The line-profile variations could not have been caused by light travel time effects akin to those observed near outburst (see Hutchings and McCall 1977), because the size of the system was too small (Table 8). Also, the ejecta had expanded to such a great size that any modulation which might be left in the remainder profiles (created by subtracting fixed ejecta profiles) would not have been resolved. Overall, it appears that the line-profile variations arose from *motions* associated with the binary.

The variations in the line-profile centroids point to projected velocities as high as 600 km s^{-1}. In Figure 6 the line profiles of Hβ and He II λ4686 can be seen to vary out to ± 1500 km s^{-1}. Such high velocities could not have arisen from the orbital motion of either star (see §VI*b*[i] and Table 8). Also, it is unlikely that the motion was associated with the rotation of either star. On the basis of Patterson's (1984) mass-radius relation, the rotational velocity of the secondary could be only 130 km s^{-1} if the rotation were synchronized with the orbit. Of course, the rotational velocity of a synchronized white dwarf would be much less. The authors conclude that the observed motions are associated with an accretion disk.

While an accretion disk is needed to explain the high-velocity emission, it is also likely that low-velocity emission was contributed by the irradiated hemisphere of the secondary. It

is possible to get a rough estimate for the strength of the He II component by assuming ionization equilibrium in the He^{++} zone created by the intercepted radiation. The intensity of He II λ4686 is given by

$$I(\text{He II } \lambda 4686) = \frac{\omega \varepsilon_{\text{eff}}(\text{He II } \lambda 4686) Q(\text{He}^+)}{16\pi^2 d^2 \alpha_B(\text{He}^+)}, \quad (24)$$

where ω is the solid angle subtended by the secondary as seen from the source of ionizing radiation, ε_{eff}(He II λ4686) is the emission coefficient for He II λ4686, $\alpha_B(\text{He}^+)$ is the case B recombination coefficient for He^{++}, $Q(\text{He}^+)$ is the rate of emission of He^+-ionizing photons by the ionizing source, and d is the distance. From Table 9, $Q(\text{He}^+) = 1.5 \times 10^{46}$ s^{-1} on day 1055. Using atomic data from Brocklehurst (1971) and Osterbrock (1974), one would predict an intensity for He II λ4686 of $(1.3\text{–}2.0) \times 10^{-12}$ ergs s^{-1} cm^{-2}, depending on the location of the ionizing source within the disk. These estimates are 2.0–3.2 times larger than the maximum He II remainder intensity (corrected for extinction) observed on day 1055. Considering the blocking effect of the disk and the complexity of the atmosphere, the discrepancy may not be surprising. More important, the prediction is large enough to suggest that the secondary contributed a significant amount of flux to the remainder profiles of the helium and hydrogen lines.

In Figures 3*g* and 3*h*, it can be seen that the radial velocities of the centroids of the remainder profiles of Hβ and He II λ4686 varied from −200 to +600 km s^{-1} on day 1055. The apparent systemic velocity of +175 km s^{-1} is in the sense of Galactic rotation (see § II*a*), and far exceeds the maximum of ~ +65 km s^{-1} observed for high-velocity stars at the same longitude (Mihalas and Binney 1981; see also § II*h*). Since the mass of the ejecta is only 10^{-4} $M_\odot$, such a velocity could not have been imparted to the system by an asymmetric outburst. Therefore, it appears likely that the redshift does not reflect the true systemic velocity, but instead is an artifact of the line-profile variations.

Considering the phasing of the continuum and velocity curves and the likelihood that the cores of the line profiles were modulated in phase with the continuum (owing to the secondary's contribution), it is probable that the blue centroid velocities were biased (see the next section). However, it might be reasonable to associate the red peak (+750 km s^{-1}) of the line-profile modulation amplitude curve (Fig. 6*c*) with the radius of material moving through a shock (hot spot) at the periphery of the disk. If this material was moving in a circular Keplerian orbit, it must have been located at a distance of 0.28 $R_\odot$ from the white dwarf (assuming an inclination of 50°). This is almost exactly equal to the expected equilibrium radius for the accretion disk (§ VI*b*[i] and Table 8), and suggests that line-profile modulations were caused by the changing view of the hot spot. The material moving at 1500 km s^{-1} should have been located at a radius of 0.07 $R_\odot$. If the He II emission seen out as far as ±4300 km s^{-1} (see § V*b*[i]) came from the same place, then the disk extended in to a radius of 0.008 $R_\odot$, i.e., close to the white dwarf (see Table 8).

It is reasonable to conclude that the remainder profiles of the hydrogen and helium emission lines consist of a broad component from the accretion disk with a core filled in partly by emission from the secondary, across all of which moves another component probably associated with a hot spot at the edge of the disk. It is not known whether or not the hot spot and the source of ionization were one and the same, especially in view of the fact that V1500 Cygni is now known to be a polar.

v) *Cause of the Variations*

In this section an effort is made to pinpoint the causes of the light and velocity variations around day 1055 (1978 July 18). The conclusions should apply to epochs subsequent to period stabilization (i.e., after 1977), but perhaps not to earlier times. For a discussion of models for the variations before 1977, the reader should refer to § II*m*(ii) and references therein.

First, it is useful to summarize the findings to this point.

1. There was a very hot (1.8×10^5 K), small (0.03 $R_\odot$) source of ionizing radiation within the binary.
2. Most of the optical continuum and a significant fraction of the remainder line emission came from the hemisphere of the secondary irradiated by the ionizing source.
3. A large fraction of the flux in the remainder line emission, particularly at high velocities, came from an accretion disk.
4. A hot spot was present at the periphery of the disk.

Critical phases for 1978 July 18 are summarized in Table 11.

The cyclical continuum variations can be attributed now to the changing aspect of the secondary. A limit to the amplitude can be predicted by assuming that the surface brightness of any point on the apparent disk was a function only of its irradiance. In this approximation, the phase law for a Lambertian reflecting sphere is applicable (see Lester, McCall, and Tatum 1979). For an inclination of 50°, the continuum would be expected to vary by 3.4 mag. In reality, the amplitude should be *lower* as a result of the adjustment of the entire atmosphere to the exposure to the primary. Another limit to the amplitude can be estimated from the range in the color temperature of the optical continuum. As discussed in § VI*b*(iii), the color temperature of the secondary on 1978 July 18 ranged from 14,000 to 17,000 K, implying a continuum variation of 0.4 mag at 4785 Å. In fact, the amplitude should be *higher* because of the weighting effect of the hottest

TABLE 11

PHASES OF EXTREMA (1978 July 18)

Parameter	Extremum	Phase	Uncertainty
Continuum flux	Maximum	−0.01	0.03
He II equivalent width	Minimum	−0.01	0.03
He II, Hβ centroid velocity	Negative	0.20	0.05
He II flux	Minimum	0.45	0.10
Continuum flux	Minimum	0.55	0.03
He II equivalent width	Maximum	0.56	0.02
He II, Hβ centroid velocity	Positive	0.62	0.05
He II flux	Maximum	0.93	0.05

parts of the apparent disk. The observed variation of the optical continuum, after correction for the contributions by the ejecta and ionizing source, was 1.3 mag, which is encompassed by the predicted upper and lower bounds. It is concluded that the attribution of the optical continuum to the secondary naturally leads to an explanation for the continuum variations consistent with the observations.

Part of the cyclical variations of the remainder line fluxes must also have been due to the changing aspect of the secondary. However, the fact that the line flux extrema occurred 0.06–0.10 cycles earlier than the continuum flux extrema suggests that another component of the line profiles, possibly that due to the hot spot (see below), may have been varying out of phase. Since the flux in He II λ4686 varied by 0.9 mag less than the continuum from the secondary (see Fig. 3*e*), the line profiles also must have contained a component which did not vary at all over the course of a cycle. Since a broad emission profile was visible at all phases, it is reasonable to identify the accretion disk as a significant source of nonvariable flux.

The night-to-night changes in the continuum and line fluxes (see also § II*b*) imply that the source irradiating the secondary was strongly and erratically variable. Along with the flickering, this would suggest a link to mass transfer, and possibly pinpoint the hot spot as the source of ionization. Therefore, it might be expected that the time scale for continuum level and amplitude changes would be longer than for line flux level changes, since the atmosphere of the secondary would require time to adjust to the change in irradiation. Figure 3 indeed shows that secular line and continuum flux changes were decoupled. Even though the He II λ4686 fluxes on July 17 and July 21 were 1.5 times lower than on July 18, the mean continuum level changed by less than 20%. As a result, the equivalent widths were systematically lower (Fig. 3*e*). Tentatively, the authors identify the mass transfer rate as the factor controlling the mean level of the line fluxes and the mean level and amplitude of the continuum.

The azimuth of the hot spot within the accretion disk can be estimated from the difference in phase between maximum centroid velocity and minimum continuum flux. The phase of maximum light is a less reliable indicator because of the distortion of the irradiated hemisphere of the secondary, and the phase of minimum velocity was biased by other sources of line radiation. It is probably reasonable to assume that maximum velocity was associated with a line of sight perpendicular to the radius vector to the hot spot, and that minimum light occurred when the observer viewed the system along a line in the vertical plane joining the center of the secondary to the hot spot. Then the angle α between the radius vector to the spot and the line joining the two stars (measured in the sense of the mass circulation) is given by

$$\alpha = \frac{\pi}{2} - 2\pi\delta - \arcsin\left[\frac{r_{\rm disk}}{a}\cos(2\pi\delta)\right], \qquad (25)$$

where $\delta = \phi(\text{Max } V) - \phi(\text{Min } F_\lambda)$, $r_{\rm disk}$ is the radius of the accretion disk, and a is the separation of the stars. The observations (Table 11) suggest that $\alpha = 54°$. In comparison, theoretical models by Flannery (1975) predict an azimuth of 62°.

To help study the phasing of cyclical light and velocity variations and the details of the line-profile changes, a scale drawing of the authors' model for V1500 Cygni is presented in Figure 8. Most of the data required to construct the diagram were taken from Table 8. The shape of the secondary (M_2) and the Roche lobe around the primary (M_1) were determined using the tables of Plavec and Kratochvil (1964). The orientation of the system as a function of phase was set by the azimuth of the hot spot, since it was assumed that maximum velocity occurred when the radius vector to the spot was perpendicular to the line of sight. The irradiation of the secondary has been drawn on the assumption that the hot spot was the source of ionizing radiation.

The model shown in Figure 8 predicts the orientation of the system at minimum and maximum line flux and minimum velocity. Minimum line flux occurred close to the phase at which the observer was looking directly at the hot spot. This suggests that line emission from the spot was being absorbed or scattered by foreground material associated with the mass stream. At the same time, a significant fraction of the line emission from the secondary would have been occulted. The observed phase of minimum represents the orientation at which the *sum* of the contributions from the secondary and hot spot was a minimum, and so lies in between lines of sight toward the rear of the secondary and the front of the hot spot. By the same token, maximum line flux occurred at a phase when the observer had the clearest views of the hot spot and the irradiated face of the secondary.

Figure 8 also demonstrates the origin of the asymmetric centroid velocity extrema. At the phase of minimum velocity, the observer had a largely clear view of line emission from the secondary, but the hot spot was probably obscured by gas in the mass transfer column or shocked downstream material in the disk. The centroid velocity would have been biased toward the red by both effects. Assuming an orbital velocity of 400 km s^{-1}, a rotational velocity of 130 km s^{-1}, and an inclination of 50°, the secondary emission profile would have been centered around -190 km s^{-1} at this time, which is close to the observed centroid minimum. On the other hand, at the phase of maximum velocity, the observer not only had a clearer view of the hot spot, but the emission from the secondary was partially occulted. As a result, the biasing effect of low-velocity emission would have been less severe. The authors feel that it is this balancing act between secondary and spot emission which is at the root of the complexities of the line-profile variations depicted in Figure 6. To explain the observations of N III emission, it is necessary for contributions to have come from the accretion disk and secondary, but *not* from the hot spot.

The model can also account for the reduced amplitude of the centroid velocity curves observed on 17 July and 21 July. When the mass transfer rate declines, the emissivities of both the hot spot and the irradiated hemisphere of the secondary should decrease. Under these circumstances, the line profiles could well be dominated by the emission from the accretion disk, so the centroids should come closest to the radial velocity of the primary and the amplitude of the centroid variations should approach 90 sin i km s^{-1} (Table 8). Indeed, Figures 3*g* and 3*h* show that remainder profile velocities

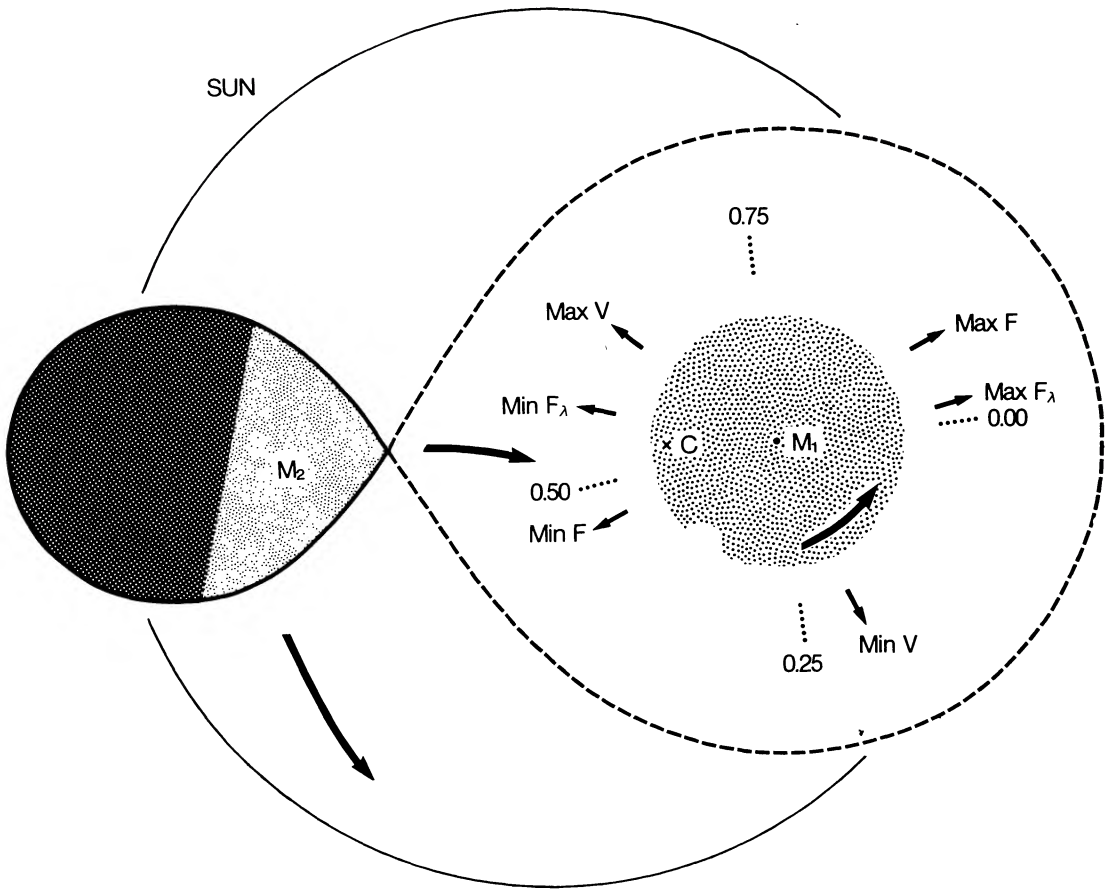

FIG. 8.—Nova V1500 Cygni in 1978, to scale, drawn as a positive. The parameters of the binary system have been taken from Table 8 and the text. The cross labeled *C* marks the center of mass, and the dashed curve delineates the Roche lobe around the primary. The large arrows point in the direction of mass motions. The small arrows around the accretion disk point toward the location of the observer at critical phases of 1978 July 18. The symbols F_λ, *F*, and *V* refer to the continuum flux, the remainder line flux, and the remainder centroid velocity, respectively. The orientation of the phase compass was set by the difference between the phases of minimum light and maximum velocity, assuming that the hot spot was the source of ionizing radiation.

generally remained within 100 km s^{-1} of zero on the nights when the activity of the system, as evidenced by the He II remainder flux, was significantly reduced.

Owing to the nature of the irradiation and the shape of the secondary, Figure 8 suggests that the continuum light curve should have a sharper maximum than minimum, and that the rise to maximum should be steeper than the fall to minimum. This is exactly what is observed in Figures 3*a* and 3*f*. Shifts in the azimuth of the hot spot might account for some of the phase jitter observed in the continuum extrema (Patterson 1979).

While the model presented for V1500 Cygni appears to be able to cope with many aspects of the authors' observations, there are still important uncertainties. First, although the centroids of Hβ and He II λ4686 varied in the same manner on 1978 July 18, with an apparent period close to that of the continuum variations, the time baseline was short enough (1.2 cycles) that the long-term persistence of the modulation and its phasing could not be demonstrated. Second, it is difficult to account for large cycle-to-cycle variations in the continuum amplitude during a night (as reported by some photometrists; see § II*b*) unless the secondary was able to adjust very rapidly (in a time of the order of one period) to changes in irradiation. Third, it is not known whether or not the period of the velocity variations was *identical* with that of the continuum variations.

VII. CONCLUSIONS

The authors have undertaken a comprehensive study of Nova V1500 Cygni in order to determine the characteristics of the ejecta and to gain some insights into the nature of the progenitor and its subsequent evolution. Previously published data have been reviewed, and new observations obtained 3 years after maximum light have been presented.

First, past work on the nova was assessed to ascertain the most probable values of critical parameters. In particular, the distance was estimated to be 1.2 ± 0.2 kpc, showing that the absolute magnitude at peak was $M_V = -10.2 \pm 0.3$.

A reanalysis of observations made by Ferland and Shields (1978*b*) between days 40 and 150 revealed that the abundances of carbon, nitrogen, oxygen, and neon in the ejecta were enhanced over the solar values by factors of 20, 60, 8, and 9, respectively. The excesses were 1.4–3.0 times lower than estimated by Ferland and Shields, both because of errors in their analysis and because of recent revisions to the atomic

data. The helium abundance was close to that found in local Galactic H II regions. The great strength of the [O III] lines 3 years after maximum light (60 times Hβ) was explained by the combination of a hard ionizing spectrum and a high density. Fine-structure lines which would normally dominate the cooling of such a metal-rich gas were saturated, so the electron temperature was a high 11,000 K.

From a comparison of radio and optical density estimates, the filling factor was estimated to be substantially less than 1.0 after about 1 month after outburst. It was found to decline with time, suggesting that the self-expansion of clumps in the ejecta was decelerating. If the effect was due to interactions with an interclump medium, the process might have been a significant source of power for the corona.

The data obtained 3 years after maximum showed that the centroid velocities of Hβ and He II λ4686 (after removal of the nebular contribution) varied periodically between -200 and $+600$ km s^{-1}, confirming the binary nature of the progenitor. The period of the velocity variations was close to that of the continuum. Pre-nova observations indicated that the secondary was an M dwarf. The progenitor appears to have been a typical cataclysmic system in which an M4 V star was transferring mass to a degenerate companion, probably a white dwarf.

From estimates for the local density, Hβ luminosity, and metal abundances, the mass of the ejecta was determined to be $(5\text{–}15)\times10^{-5}\ M_\odot$. Models of novae as a function of speed, metallicity, and ejecta mass suggested that the mass of the white dwarf was close to the Chandrasekhar limit. This offers a natural explanation for the uniqueness of the eruption. The great enhancements of carbon, oxygen, and neon in the ejecta indicated that, in addition to the accreted envelope, material from the white dwarf core was involved in the outburst, contributing about 25% of the mass of the ejecta. The fact that the helium abundance was close to the cosmic value demonstrated that the white dwarf was rich in carbon, oxygen, and neon, but deficient in hydrogen and helium. The huge abundance of nitrogen indicated that the nova explosion was powered by the CNO cycle.

Ejecta emission 3 years after the maximum showed that the source of ionizing radiation was very hot (180,000 K) and small ($0.07\ R_\odot$). The breadth of the Hβ and He II line profiles demonstrated the existence of an accretion disk, and the amplitude of the velocity variations suggested the presence of a hot spot on the periphery. Most of the optical continuum appeared to have come from the hemisphere of the secondary irradiated by the source of ionizing radiation. Thus, the periodic variations could be explained as a manifestation of the changing view of the secondary. In addition, the secondary probably contributed a considerable amount of the flux in Hβ and He II λ4686. Periodic variations in the emission-line fluxes appeared to have been a result of the changing aspect of the secondary and the anisotropy in optical depth around the hot spot. The changing balance between the secondary and spot contributions to the emission lines was probably responsible in large part for the asymmetry in the centroid velocity extrema.

Further observations would be valuable for checking the conclusions of this paper. One advantage now is that the ejecta have expanded to the point at which observations of the central object can be made with enough spatial resolution to exclude much of the emission. However, inferences about central object properties based on ejecta emission could be risky because of the long recombination time scale.

Infrared spectroscopy of the ejecta would be useful for checking the importance of fine-structure lines to the evolution of the cooling. By 1984 the density should have declined to the critical value for the $^3P_2$ level of O^{++}, so the strength of the optical [O III] lines should have begun to decline relative to Hβ. Long-term observations of continuum fluxes and line centroid velocities are needed to assess the stability of the phasing, in order to determine whether or not phase shifts can be attributed to changes in the azimuth of the hot spot. More extensive observations of the correlation between continuum and line fluxes are needed to study how the secondary responds to changes in irradiation.

Potentially, observations of the flickering could measure the fraction of the continuum contributed by the secondary. The model presented here predicts that the amplitude of flickering on time scales short enough that the secondary has no time to react to the changes in irradiation should be inversely proportional to the continuum flux.

The authors are grateful for the assistance provided by the staffs of McDonald Observatory and Mount Stromlo and Siding Spring Observatories. In addition, thanks are conveyed to Anthony Dixon for his aid with the reductions, and to Gary Ferland, Peter Martin, Stefan Mochnacki, Slawek Ruciński, and Brian Warner for helpful discussions. M. L. M. thanks the Natural Sciences and Engineering Research Council of Canada for the financial support which made this work possible.

APPENDIX

THE DATA FOR THE ABUNDANCE ANALYSIS

The line ratios required for the abundance study were extracted from FS78 and Ferland (1978*b*), the latter of which were published recently by Ferland, Lambert, and Woodman (1986*a*). In the process, several errors were discovered in these works and that of Ferland (1978*a*). Since the data are unique and have such an important impact on studies of the nova phenomenon and the evolution of galaxies, these deficiencies are summarized here to ensure that future investigations are not misdirected.

1. The label on the y-axis of Figure 4 in FS78 is incorrect. The plot is nonlogarithmic.

2. The reddening corrections listed in Tables 3.1, 3.2, and 3.3 of Ferland (1978*b*) were derived using $E(B-V)=0.51$, not $E(B-V)=0.53$ (as stated in the preface).

3. The values of I([O III] λ5007)/I([O III] λ4363) computed from Table 3.3 of Ferland (1978*b*) are inconsistent with those plotted in Figure 4 of FS78. After measuring Figures 1, 2, 3, and 5, it was concluded that the values of F([O III] λ4363)/F(Hβ)

given by Ferland (1978*b*) are in error. They appear to have been computed directly from the dereddened ratios I([O III] λ5007)/I([O III] λ4363) and the reddened ratios F([O III] λ5007)/F(Hβ).

4. The values of F(He I λ5876)/F(Hβ) and F(He I λ6678)/F(Hβ) plotted in Figure 4 of Ferland (1978*a*) and used in the helium abundance analysis in Table 1 of that paper are inconsistent with the values listed in both Table 1 of FS78 and Table 3.1 of Ferland (1978*b*). They are low by a factor equal to the ratio of wavelengths. It is likely that the flux ratios were computed from ratios of line peaks without compensation for the variation of line width with wavelength.

5. In Table 1 of FS78, the "corrected" ratio I(He II λ5412)/I(Hβ) is greater than the "observed" ratio. The only way of reconciling Figure 6 of Ferland (1978*a*) with the data is to recognize the "corrected" intensities as being accurate. The "observed" values in the table appear to have been computed from the "corrected" values by applying the reddening correction in the wrong direction.

6. In Figure 13 of FS78, the ordinate labels are too high by a factor of 10.

With the aid of the error identifications above, the *observed* line ratios relevant to the abundance study were derived from the following sources:

1. [Ne V] λ3426/[Fe VII] λ6087: FS78 (p. 180), using reddening corrections from Miller and Mathews (1972) for $E(B-V) = 0.51$.
2. [Ne III] λ3869/Hβ: FS78 (Fig. 6), and F([O III] λ5007)/F(Hβ).
3. C III λ4187/Hβ: FS78 (Fig. 13), divided by 10.
4. C II λ4267/Hβ: FS78 (Fig. 12).
5. [O III] λ4363/Hβ: Ferland (1978*b*, Table 3.3), multiplied by 0.940/1.276.
6. [O III] λ5007/Hβ: Ferland (1978*b*, Table 3.3).
7. He II λ5412/Hβ: FS78 ("Reddening-corrected Intensity" in Table 1), using the reddening corrections in Table 3.1 of Ferland (1978*b*).
8. [N II] λ5755/Hβ: Ferland (1978*b*, Table 3.3).
9. He I λ5876/Hβ: Ferland (1978*b*, Table 3.1).
10. [O I] λ6300/Hβ: Ferland (1978*b*, Table 3.3).
11. He I λ6678/Hβ: Ferland (1978*b*, Table 3.1).
12. [O II] λ7325/Hβ: Ferland (1978*b*, Table 3.3).

Subsequent to the completion of this work, Ferland, Lambert, and Woodman (1986*b*) confirmed that the tabulations of F([O III] λ4363)/F(Hβ) in Ferland (1978*b*) and Ferland, Lambert, and Woodman (1986*a*) were in error. Mistakenly, the *reddening-corrected* values were listed, so that the *observed* values were actually a factor of 1.276 lower. This accounts for most of the discrepancy noted above. If this is the only error, then the values of F([O III] λ4363)/F(Hβ) adopted for use in the abundance analysis here were 6% too low, suggesting that temperatures were slightly underestimated.

To assess the effect of a 6% upward revision to F([O III] λ4363)/F(Hβ), the temperature-density analysis was repeated using appropriately revised line ratios. As expected, temperatures increased systematically, but by only 200 K. Densities increased by only 0.005 dex. The ratio $X(O^{++})/X(Ne^{++})$ increased by 1%, while $X(O^{++})/X(He^{+})$ decreased by 6%. All of the changes lie within the range of uncertainty associated with these quantities. Since ratios of emission coefficients for recombination lines are not significantly altered by the changes in temperature and density, the helium abundance is unaffected. However, the metal abundances decrease in step with $X(O^{++})/X(He^{+})$, i.e., by 0.03 dex. This change is smaller than the range of abundance determinations in Table 6, and is much below the estimated errors given in Table 7. Thus, no alteration of the paper is necessary.

REFERENCES

Aldrovandi, S. M. V., and Péquignot, D. 1973, *Astr. Ap.*, **25**, 137.
Alksne, Z., and Platais, I. 1975, *Astr. Tsirk.*, No. 889, p. 8.
Baluja, K. L., Burke, P. G., and Kingston, A. E. 1981, *J. Phys. B*, **14**, 119.
Barnes, T. G. 1976, *M.N.R.A.S.*, **177**, 53P.
Barnes, T. G., and Evans, D. S. 1976, *M.N.R.A.S.*, **174**, 489.
Barnes, T. G., Evans, D. S., and Parsons, S. B. 1976, *M.N.R.A.S.*, **174**, 503.
Beall, J. H., Knight, F. K., Smith, H. A., Wood, K. S., Lebofsky, M., and Rieke, G. 1984, *Ap. J.*, **284**, 745.
Beardsley, W. R., King, M. W., Russell, J. L., and Stein, J. W. 1975, *Pub. A.S.P.*, **87**, 943.
Becker, H. J., and Duerbeck, H. W. 1980, *Pub. A.S.P.*, **92**, 792.
Binette, L. 1983, Ph.D. thesis, Australian National University.
Boyarchuk, A. A. 1977, in *IAU Colloquium 42, The Interaction of Variable Stars with Their Environment*, ed. R. Kippenhahn, J. Rahe, and W. Strohmeier (Bamberg: Schadel), p. 274.
Boyarchuk, A. A., and Gershberg, R. E. 1977, *Soviet Astr.—AJ*, **21**, 275.
Brocklehurst, M. 1971, *M.N.R.A.S.*, **153**, 471
_____. 1972, *M.N.R.A.S.*, **157**, 211.
Buscombe, W., and de Vaucouleurs, G. 1955, *Observatory*, **75**, 170.
Cameron, A. G. W. 1982, in *Essays in Nuclear Astrophysics*, ed. C. A. Barnes, D. D. Clayton, and D. N. Schramm (Cambridge: Cambridge University Press), p. 23.
Campbell, B. 1975, *IAU Circ.*, No. 2839.
_____. 1976, *Ap. J. (Letters)*, **207**, L41.
Chlebowski, T., and Kaluzny, J. 1987, *IAU Circ.*, No. 4413.
Cohen, J. G. 1985, *Ap. J.*, **292**, 90.
Colvin, J. D., Van Horn, H. M., Starrfield, S. G., and Truran, J. W. 1977, *Ap. J.*, **212**, 791.
de Vaucouleurs, G., and de Vaucouleurs, A. 1984, *Sky and Tel.*, **68**, 412.
de Vegt, C., and Gehlich, U. 1975, *IAU Circ.*, No. 2837.
de Vegt, C., Gehlich, U. K., and Kohoutek, L. 1975, *IAU Circ.*, No. 2826.
Duerbeck, H. W. 1987, *Space Sci. Rev.*, **45**, 1.
Duerbeck. H. W., and Wolf, B. 1977, *Astr. Ap. Suppl.*, **29**, 297.
Efimov, Yu. S., Narizhnaya, N. V., and Shakhovskoi, N. M. 1977, *Soviet Astr.—AJ*, **21**, 278.
Eissner, W., and Seaton, M. J. 1974, *J. Phys. B*, **7**, 2533.
Elitzur, M., Ferland, G. J., Mathews, W. G., and Shields, G. A. 1983, *Ap. J.*, **272**, L55.
Ennis, D., Becklin, E. E., Beckwith, S., Elias, J., Gatley, I., Mathews, K., Neugebauer, G., and Willner, S. P. 1977, *Ap. J.*, **214**, 478.
Fabian, A. C., and Pringle, J. E. 1977, *M.N.R.A.S.*, **180**, 749.
Fehrenbach, Ch., and Andrillat, Y. 1976, *Astr. Ap.*, **52**, 123.
Ferland, G. J. 1977*a*, *Ap. J. (Letters)*, **212**, L21.
_____. 1977*b*, *Ap. J.*, **215**, 873.
_____. 1978*a*, *Ap. J.*, **219**, 589.
_____. 1978*b*, Ph.D. thesis, University of Texas at Austin.

Ferland, G. J. 1979, *Ap. J.*, **231**, 781.
_____. 1980, *Ap. J.*, **236**, 847.
Ferland, G. J., Lambert, D. L., McCall, M. L., Shields, G. A., and Slovak, M. H. 1982, *Ap. J.*, **260**, 794.
Ferland, G. J., Lambert, D. L., and Woodman, J. H. 1977, *Ap. J.*, **213**, 132.
_____. 1986*a*, *Ap. J. Suppl.*, **60**, 375.
_____. 1986*b*, *Ap. J. Suppl.*, **62**, 939.
Ferland, G. J., and Shields, G. A. 1978*a*, *Ap. J. (Letters)*, **224**, L15.
_____. 1978*b*, *Ap. J.*, **226**, 172 (FS78).
Fischer, L. 1976, *M.N.R.A.S.*, **177**, 67P.
Flannery, B. P. 1975, *M.N.R.A.S.*, **170**, 325.
Gallagher, J. S., and Ney, E. P. 1976, *Ap. J. (Letters)*, **204**, L35.
Grasdalen, G. L., and Joyce, R. R. 1976, *Nature*, **260**, 187.
Green, R. F. 1980, *Ap. J.*, **238**, 685.
Hummer, D. G., and Mihalas, D. 1970, *M.N.R.A.S.*, **147**, 339.
Hutchings, J. B. 1972, *M.N.R.A.S.*, **158**, 177.
_____. 1979, *Ap. J.*, **230**, 162.
Hutchings, J. B., Bernard, J. E., and Margetish, L. 1978, *Ap. J.*, **224**, 899.
Hutchings, J. B., Bernard, J. E., Margetish, L., and McCall, M. 1978, *Pub. Dom. Ap. Obs.*, **15**, 73.
Hutchings, J. B., and McCall, M. L. 1977, *Ap. J.*, **217**, 775.
Isobe, S., Kosai, H., Hara, H., Fukaya, R., and Adachi, Y. 1975, *Pub. Astr. Soc. Japan*, **27**, 619.
Jacoby, G. H., Hunter, D. A., and Christian, C. A. 1984, *Ap. J. Suppl.*, **56**, 257.
Jeffers, S., and Weller, W. 1975, *IAU Circ.*, No. 2839.
Kawara, K., Maihara, T., Noguchi, K., Oda, N., Sato, S., Oishi, M., and Iijima, T. 1976, *Pub. Astr. Soc. Japan*, **28**, 163.
Kemp, J. C., King, R., Parker, T. E., and Johnson, P. E. 1979, *Pub. A.S.P.*, **91**, 214.
Kemp, J. C., and Rudy, R. J. 1976, *Ap. J. (Letters)*, **203**, L131.
Kemp, J. C., Sykes, M. V., and Rudy, R. J. 1977, *Ap. J. (Letters)*, **211**, L71.
Kruszewski, A., Semeniuk, I., and Duerbeck, H. W. 1983, *Acta Astr.*, **33**, 339.
Lang, K. R. 1980, *Astrophysical Formulae* (Berlin: Springer), p. 559.
Lanning, H. H., and Semeniuk, I. 1981, *Acta Astr.*, **31**, 175.
Lester, T. P., McCall, M. L., and Tatum, J. B. 1979, *J.R.A.S. Canada*, **73**, 233.
MacDonald, J. 1983, *Ap. J.*, **267**, 732.
McFarlane, M. J. 1969, *Pub. A.S.P.*, **81**, 46.
McCall, M. L. 1984, *M.N.R.A.S.*, **207**, 801.
McLean, I. S. 1976, *M.N.R.A.S.*, **176**, 73.
Mendoza, C. 1983, in *IAU Symposium 103, Planetary Nebulae*, ed. D. R. Flower (Dordrecht: Reidel), p. 143.
Mihalas, D., and Binney, J. 1981, *Galactic Astronomy* (2d ed.; San Francisco: Freeman), p. 380.
Miller, J. S., and Mathews, W. G. 1972, *Ap. J.*, **172**, 593.
Moore, C. E. 1972, *A Multiplet Table of Astrophysical Interest: Revised Edition* (Washington, DC: National Bureau of Standards).
Nauenberg, M. 1972, *Ap. J.*, **175**, 417.
Neff, J. S., Smith, V. V., and Ketelsen, D. A. 1978, *Ap. J. Suppl.*, **38**, 89.
Osada, K. 1975, *IAU Circ.*, No. 2826.
Osterbrock, D. E. 1974, *Astrophysics of Gaseous Nebulae* (San Francisco: Freeman).
Osterbrock, D., and Flather, E. 1959, *Ap. J.*, **129**, 26.
Patterson, J. 1978, *Ap. J.*, **225**, 954.
_____. 1979, *Ap. J.*, **231**, 789.
_____. 1984, *Ap. J. Suppl.*, **54**, 443.
Peimbert, M., and Sarmiento, A. 1984, *Astr. Express*, **1**, 97.
Peimbert, M., Torres-Peimbert, S., and Rayo, J. F. 1978, *Ap. J.*, **220**, 516.
Plavec, M., and Kratochvil, P. 1964, *Bull. Astr. Inst. Czechoslovakia*, **15**, 165.
Rosino, L., and Tempesti, P. 1977, *Soviet Astr.—AJ*, **21**, 291.
Samus, N. N. 1975, *IAU Circ.*, No. 2826.
Schild, R. E. 1977, *A.J.*, **82**, 337.
Schmidt, G. D., Smith, P., and Elston, R. 1987, *IAU Circ.*, No. 4415.
Schmidt-Kaler, Th. 1982, in *Landolt-Börnstein, New Ser.*, Vol. **2b**, ed. K. Schaifers and H. H. Voigt (Berlin: Springer), p. 1.
Seaquist, E. R., Duric, N., Israel, F. P., Spoelstra, T. A. T., Ulich, B. L., and Gregory, P. C. 1980, *A.J.*, **85**, 283.
Seaton, M. J. 1975, *M.N.R.A.S.*, **170**, 475.
_____. 1978, in *IAU Symposium 76, Planetary Nebulae*, ed. Y. Terzian (Dordrecht: Reidel), p. 131.
Semeniuk, I., Kruszewski, A., Schwarzenberg-Czerny, A., Chlebowski, T., Mikolajewski, M., and Wolczyk, J. 1977, *Acta Astr.*, **27**, 301.
Shenavrin, V. I., Moroz, V. I., and Liberman, A. A. 1977, *Soviet Astr.—AJ*, **21**, 358.
Shields, G. A., and Ferland, G. J. 1978, *Ap. J.*, **225**, 950.
Stone, R. P. S. 1977, *Ap. J.*, **218**, 767.
Storey, P. J. 1981, *M.N.R.A.S.*, **195**, 27P.
Tempesti, P. 1975, *IAU Circ.*, No. 2834.
_____. 1979, *Astr. Nach.*, **300**, 51.
Tomkin, J., Woodman, J., and Lambert, D. L. 1976, *Astr. Ap.*, **48**, 319.
Tull, R. G., Vogt, S. S., and Kelton, P. W. 1979, *Proc. SPIE*, **172**, 90.
Uomoto, A. K. 1981, Ph.D. thesis, University of Texas at Austin.
Warner, B. 1973, *M.N.R.A.S.*, **162**, 189.
_____. 1976, in *IAU Symposium 73, Structure and Evolution of Close Binary Systems*, ed. P. Eggleton, S. Mitton, and J. Whelan (Dordrecht: Reidel), p. 85.
Williams, R. E., and Ferguson, D. H. 1983, in *IAU Colloquium 72, Cataclysmic Variables and Related Objects*, ed. M. Livio and G. Shaviv (Dordrecht: Reidel), p. 97.
Wu, C.-C., and Kester, D. 1977, *Astr. Ap.*, **58**, 331.
Young, P. J., Corwin, H. G., Jr., Bryan, J., and de Vaucouleurs, G. 1976, *Ap. J.*, **209**, 882.

CATHERINE M. LANCE: Department of Astrophysics, Oxford University, South Parks Road, Oxford, England OX1 3NP

MARSHALL L. MCCALL: David Dunlap Observatory, University of Toronto, Box 360, Richmond Hill, Ontario L4C 4Y6, Canada

ALAN K. UOMOTO: Department of Physics and Astronomy, Johns Hopkins University, Baltimore, MD 21218